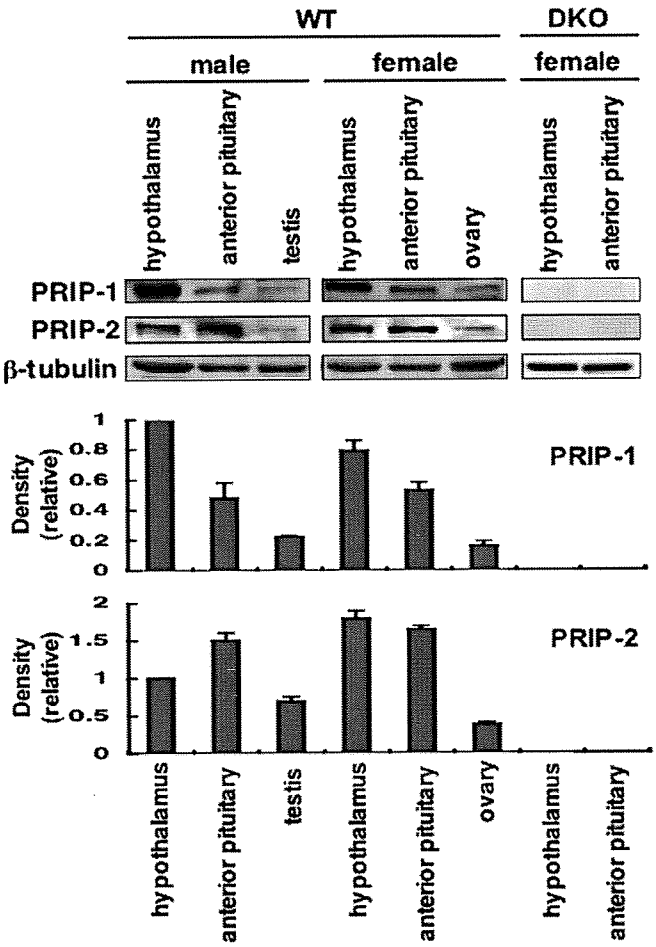

FIG. 4. The expression of PRIP-1 and -2. Tissue extracts of hypothalamus, pituitary glands, testis, and ovaries were prepared from WT mice at the age of 3 mo by homogenization with a Teflon pestle, and at a protein concentration of 20 μg each was separated by SDS-PAGE, followed by immunoblotting with antibodies against PRIP-1 and PRIP-2, with β-tubulin as a control. Samples from DKO mice were also prepared as negative control. The density of individual bands normalized with β-tubulin were represented relative to that observed with male hypothalamus. Blots shown are of typical, and the graphs show the summary of four independent experiments (mean ± SEM).

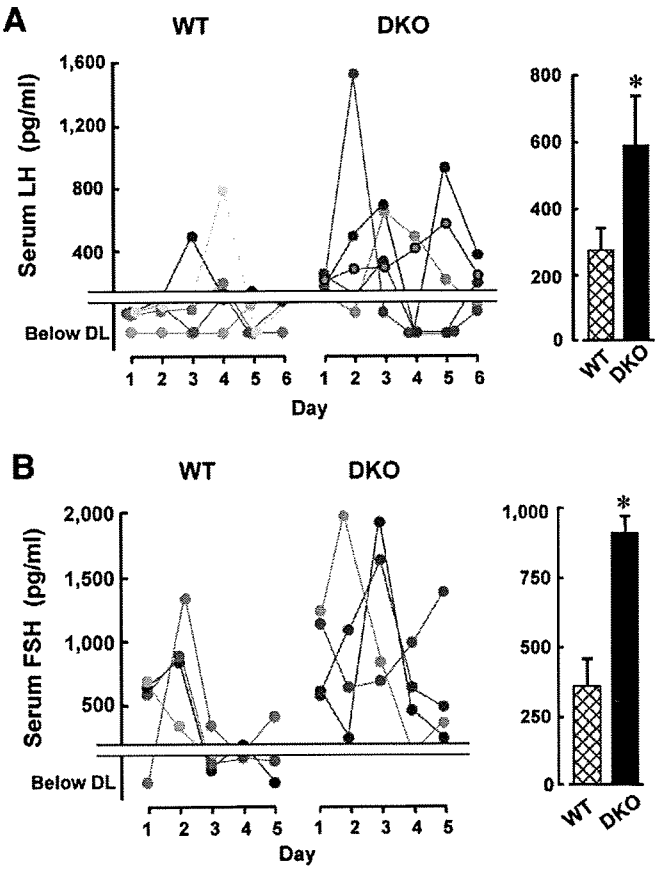

FIG. 5. Serum gonadotropin levels. Blood samples were taken from five WT and DKO females at the age of 3 mo for 5 or 6 consecutive days for FSH or LH, respectively, and their serum levels of LH (**A**) and FSH (**B**) were measured by ELISA. Each color on the graph indicates the values of individual mice. The histograms shown on the right represent the average serum gonadotropin levels measured in the experiment, but values below the detectable level (DL; less than 200 pg/ml for LH and FSH) were omitted from the calculation. Data show the means ± SEM for four to five mice each (Student *t*-test, $*P < 0.05$).

respectively, were identified. There was little difference in LHR or FSHR expression levels in the ovary between WT and DKO mice (Fig. 8C).

DISCUSSION

The present study was initiated by the observation that DKO mice exhibited a decreased number of pups per litter and fewer litters. Higher serum levels of the gonadotropins LH and FSH were observed with DKO females, and the increased estrous days were also shown in the DKO by histological analysis of vaginal smears. In humans, there are some clinical observations that hypersecretion of LH impairs fertility in females by the disruption of ovarian function or maintenance of pregnancy [23–25]. Elevated FSH is also associated with reproductive impairment. Increasing basal FSH is related to a shorter follicular phase [26–28] and cycle length [29–31] in aging females before menopause transition. Elevated basal levels of gonadotropins lead to reproductive defects; however, the mechanisms have remained obscure because of the multiple causes of female reproductive disorders associated with increased LH and/or FSH.

The hierarchical HPG axis is central to gonadohormone secretion in conjunction with positive and negative feedback mechanisms. The impairment of progesterone biogenesis from cholesterol in ovaries of DKO mice might be a primary cause for higher serum levels of gonadotropins mediated by the negative feedback loop. However, this notion attributed to progesterone biogenesis would be unlikely because the explant of the pituitary glands from DKO mice secreted more LH, independent of the amount of progesterone, and the ovary contains less PRIP than the hypothalamus and pituitary gland. The upregulation of GnRH secretion in DKO mice might be the cause for the higher levels of LH and FSH in accordance with the hierarchy, but this could not be experimentally qualified because it is difficult to measure serum levels of GnRH streaming in the hypophysial portal system. GnRH neurons were reported to be modulated by activities of $GABA_A$ receptors [32], the properties of which have been altered in DKO mice [18, 33]. In cases of either dependence on or independence of GnRH, the upregulation of secretion from pituitary glands would be more probable. Total contents of LH and FSH in the pituitary lobes was decreased in DKO mice, but the mRNA levels remained constant, suggesting that the

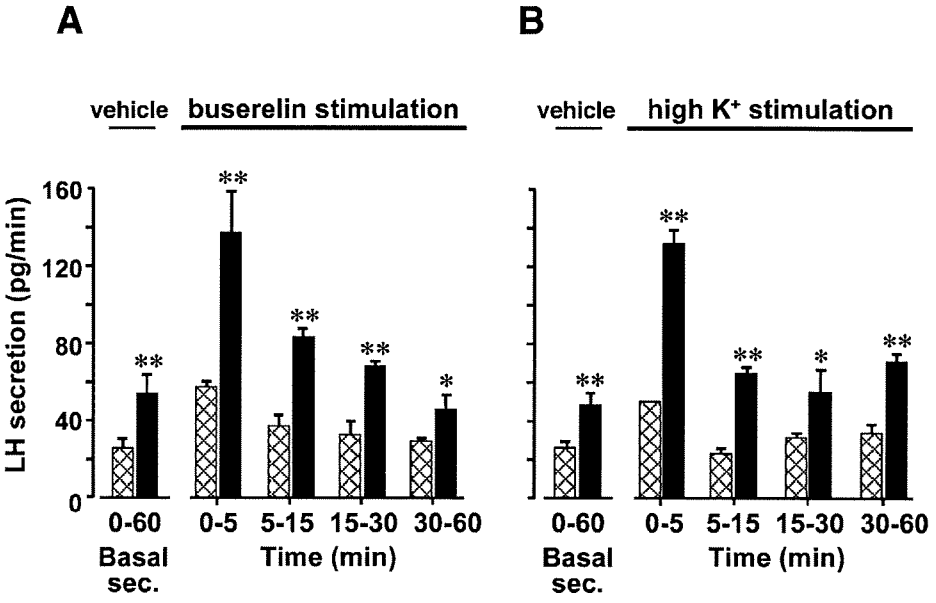

FIG. 6. LH secretion from the explant of anterior pituitary gland. Anterior pituitary glands from WT (cross-hatched bars) and DKO (black bars) mice at the age of 3 mo were cultured. The medium was collected and replenished with the same volume of fresh medium at 5, 15, 30, and 60 min in the presence of 40 nM buserelin (**A**) or high K^+ solution (**B**), and the medium without any stimulation was also collected after 60 min of incubation as the basal secretion (Basal sec.). LH levels secreted in the media were measured by ELISA and are represented in picograms per minute of incubation. Graph shows the mean ± SEM (n = 5, Student *t*-test, $*P < 0.05$, $**P < 0.01$; significant difference from those observed with WT).

constitutive upregulation of gonadotropin secretion results in decreased intrapituitary level of gonadotropins. Overall, upregulation of the secretion of LH and FSH from the pituitary glands appears to be the characteristic acquired by DKO mice. Isolated lobes of pituitary glands secreted more LH in response to both buserelin, an analog of GnRH, and high K^+ solution. Buserelin binds to the GnRH receptor of pituitary gonadotrophs, activating GnRH signaling to trigger Ca^{2+} release from storage sites through the action of $Ins(1,4,5)P_3$ following PLCβ activation [34–37], which would be followed by storage-operated Ca^{2+} influx [34, 35]. On the other hand, high K^+ solution bypasses the signaling mediated by receptor/$Ins(1,4,5)P_3$, but directly activates voltage-dependent Ca^{2+} influx. DKO pituitary lobes secreted more LH in a similar manner, independent of the type of stimulation, indicating that PRIP is actually related to the events after the increase of Ca^{2+} concentration. Furthermore, basal constitutive secretion without any stimulation was also higher in DKO lobes, indicating the independence of GnRH and the associated changes in intracellular Ca^{2+}, apart from pulsatile secretion of LH observed in vivo [38, 39]. FSH secretion was also upregulated in DKO mice. It appears that the pituitary gonadotrophs of DKO mice potentially secreted more gonadotropins, rather than that the higher serum levels of gonadotropins in DKO mice are solely dependent on the higher secretion of GnRH. Several studies reported that LH and FSH are secreted via different respective pathways after their biosynthesis [39, 40]. These reports and the results observed with DKO mice suggest that

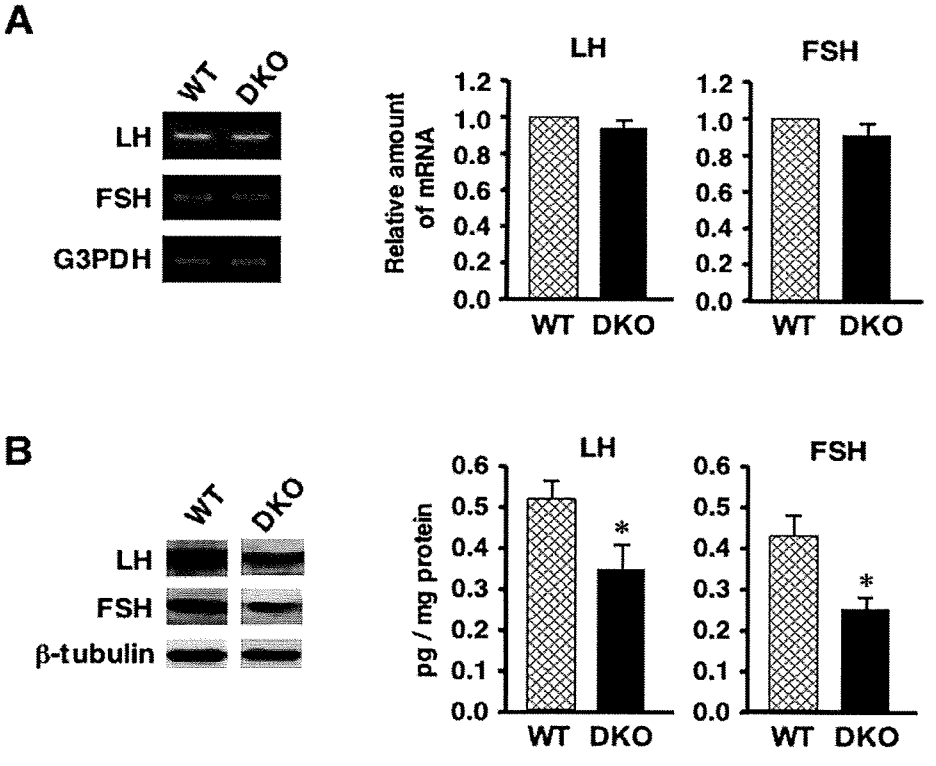

FIG. 7. The expressions of LH and FSH in anterior pituitary gland. **A**) Total RNA, prepared from the anterior pituitary gland of 3-mo-old WT and DKO mice, were subjected to RT-PCR with appropriate primers, described in *Materials and Methods*. Equivalent use of RNA was confirmed by the amplification of glyceraldehyde-3-phosphate dehydrogenase (G3PDH). Graphs show the quantification of LH and FSH mRNA levels. Each amount of mRNA obtained from quantitative RT-PCR analysis was normalized with that of individual 18s ribosomal RNA and represented relative to that of WT. Messenger RNA samples prepared from three mice were analyzed, done in triplicate (mean ± SEM). **B**) Immunoblotting was performed using 20 μg of the cell extracts from the anterior pituitary gland of both genotypes by antibodies against β-subunit of LH and FSH, and by β-tubulin as a control. Graphs indicate the amount of LH and FSH in pituitary extracts. Extracts from the anterior pituitary gland of 3-mo-old WT and DKO mice were used to measure with a respective ELISA kit. The amount of LH and FSH was represented in picograms per milligram of total protein. Values are the mean ± SEM of three independent experiments (n = 3, Student *t*-test, $*P < 0.05$).

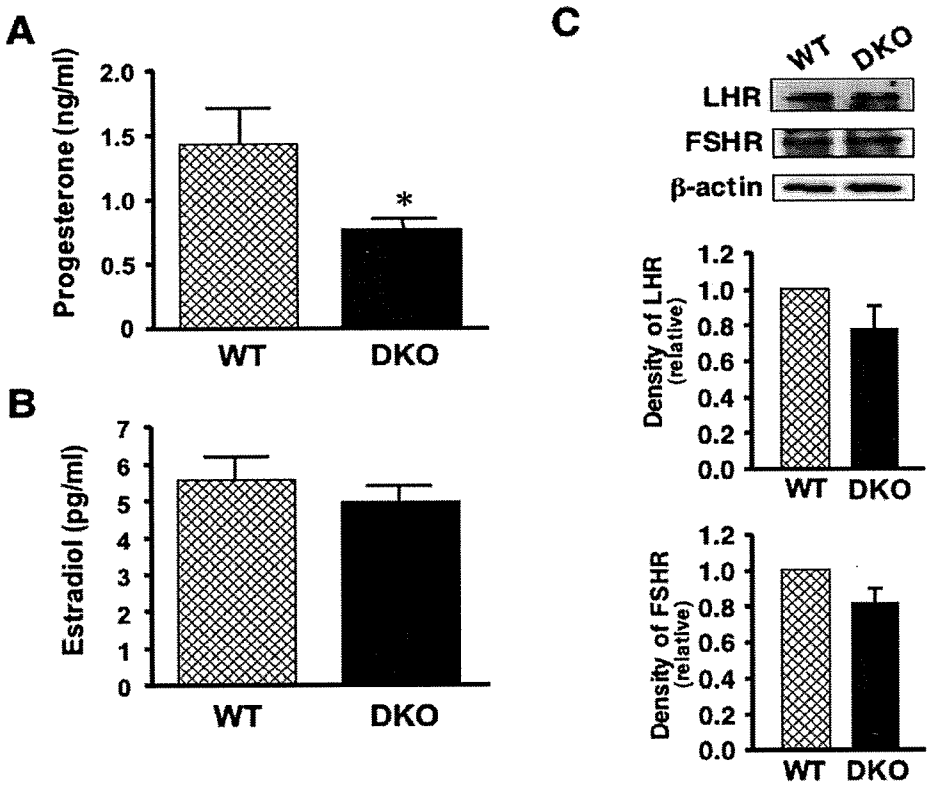

FIG. 8. Serum levels of sex steroid hormones and the expression of receptors for gonadotropins in ovary extracts. The same serum samples as for the assays shown in Figure 5 were used for the measurement of progesterone (**A**) and 17β-estradiol (**B**) levels by ELISA. The day-by-day changes of the hormones were not displayed, but the average of the measurements, omitting those below DL, is shown as the mean ± SEM of 12–20 serum samples for each genotype. $*P < 0.05$. WT and DKO ovary extracts was analyzed for gonadotropin receptors by immunoblotting using the indicated primary antibodies (**C**). The density was normalized with that of β-actin and was represented relative to that observed with WT. Graphs show the summary of three independent immunoblots (mean ± SEM).

PRIP plays an inhibitory role in the events related to granules or dense-core vesicle exocytosis in both a constitutive and facilitated manners. Thus, PRIP deficiency would result in the increased secretion of gonadotropins, which reminded us of our previous publication in which PRIP-1 KO mice showed higher serum levels of insulin [41].

In addition to SNARE proteins and synaptotagmins, many molecules, including small G proteins (rab) and their regulatory proteins (GAP, GEF, rabphilin, RIM, etc.), UNC13 (also known as Munc-13), and STXBP (also known as Munc–18), are implicated in vesicular fusion processes [42–44]. Among these molecules, one candidate to work with PRIP in a competitive manner would be CADPS (Ca^{2+}-dependent activator proteins for secretion, also known as CAPS comprising CAPS1 and 2), which was first identified as a molecule to activate Ca^{2+}-triggered dense-core vesicle exocytosis in permeable neuroendocrine cells [45, 46]. The precise molecular mechanisms enhancing exocytosis remain to be elucidated, but CADPS activity depends upon prior ATP-dependent priming, during which phosphatidylinositol-4,5-phosphate synthesis occurs. Following synthesis of the lipid, CADPS functions to enhance Ca^{2+}-dependent dense-core vesicle exocytosis as the binding protein via the PH domain [47]. As described earlier, PRIP also shares the PH domain in the domain organization, and X/Y barrel acts as a PLC-mimicking domain that lacks catalytic activity, but could accommodate the phosphoinositides (results not shown). A recent report indicated that CADPS functions not only in Ca^{2+} dependently, but also with constitutive exocytosis downstream of vesicle docking [48]. Furthermore, rabphilin could also be a candidate to work with PRIP because the molecule is reported to bind phosphatidylinositol-4,5-phosphate via its C2 domain [49, 50].

FSH stimulates follicle development, leading to 17β-estradiol synthesis. This elevated level of 17β-estradiol then results in an LH surge in a positive-feedback manner, followed by ovulation. LH also stimulates progesterone release; however, decreased levels of progesterone and little difference in 17β-estradiol were observed in DKO mice, although gonadotropin levels were elevated. No apparent difference in the number and histology of corpus luteum was observed between two genotypes. One possibility to explain this contradiction is that the expressions of LHR and FSHR are lower in DKO ovaries, caused by their down-regulation because of constant hyperstimulation. The result assessed by immunoblotting appears to exclude this possibility; however, this included the receptors of whole tissue extracts, not only functional receptors on the cell surface. Furthermore, signaling pathways following ligand binding might be down-regulated in DKO mice.

Smaller uteri were observed in 6-mo-old DKO females. Because little difference in the size of the uterus between two genotypes was observed in mice up to the age of at least 12 wk, retardation in the maturation step of the uterus occurs after puberty. 17β-Estradiol is involved in the development and maintenance of the uterus, and progesterone is involved in maintaining the uterus condition for fertility. A decreased level of progesterone might lead to a smaller uterus and reduce fertility. A previous report indicated that transgenic LHβCTP females in which LH was elevated presented a hormone imbalance causing a defect in uterine receptivity, resulting in the induction of midgestation pregnancy failure [51]. Such defects might also occur in these DKO females because of elevated LH levels.

This study introduced a novel molecule named PRIP into the reproductive system, probably through regulating gonadotropin levels, but further studies are apparently required to explore how PRIP is involved in regulation of the gonadotropin level and the reproduction system.

ACKNOWLEDGMENT

We thank Prof. Ken-ichirou Morohashi (Faculty of Medical Science, Kyushu University) for valuable advice in examination of the estrous cycle.

REFERENCES

1. Kanematsu T, Takeya H, Watanabe Y, Ozaki S, Yoshida M, Koga T, Iwanaga S, Hirata M. Putative inositol 1,4,5-trisphosphate binding proteins in rat brain cytosol. J Biol Chem 1992; 267:6518–6525.
2. Kanematsu T, Misumi Y, Watanabe Y, Ozaki S, Koga T, Iwanaga S, Ikehara Y, Hirata M. A new inositol 1,4,5-trisphosphate binding protein similar to phospholipase C-δ1. Biochem J 1996; 313:319–325.
3. Kanematsu T, Yoshimura K, Hidaka K, Takeuchi H, Katan M, Hirata M. Domain organization of p130, PLC-related catalytically inactive protein, and structural basis for the lack of enzyme activity. Eur J Biochem 2000; 267:2731–2737.
4. Yoshida M, Kanematsu T, Watanabe Y, Koga T, Ozaki S, Iwanaga S, Hirata M. D-*myo*-inositol 1,4,5-trisphosphate-binding proteins in rat brain membranes. J Biochem 1994; 115:973–980.
5. Matsuda M, Kanematsu T, Takeuchi H, Kukita T, Hirata M. Localization of a novel inositol 1,4,5-trisphosphate binding protein, p130 in rat brain. Neurosci Lett 1998; 257:97–100.
6. Takeuchi H, Kanematsu T, Misumi Y, Yaakob HB, Yagisawa H, Ikehara Y, Watanabe Y, Tan Z, Shears SB, Hirata M. Localization of a high-affinity inositol 1,4,5-trisphosphate/inositol 1,4,5,6-tetrakisphosphate binding domain to the pleckstrin homology module of a new 130 kDa protein: characterization of the determinants of structural specificity. Biochem J 1996; 318:561–568.
7. Takeuchi H, Kanematsu T, Misumi Y, Sakane F, Konishi H, Kikkawa U, Watanabe Y, Katan M, Hirata M. Distinct specificity in the binding of inositol phosphates by pleckstrin homology domains of pleckstrin, RAC-protein kinase, diacylglycerol kinase and a new 130 kDa protein. Biochim Biophys Acta 1997; 1359:275–285.
8. Takeuchi H, Oike M, Paterson HF, Allen V, Kanematsu T, Ito Y, Erneux C, Katan M, Hirata M. Inhibition of Ca^{2+} signalling by p130, a phospholipase-C-related catalytically inactive protein: critical role of the p130 pleckstrin homology domain. Biochem J 2000; 349:357–368.
9. Harada K, Takeuchi H, Oike M, Matsuda M, Kanematsu T, Yagisawa H, Nakayama KI, Maeda K, Erneux C, Hirata M. Role of PRIP-1, a novel Ins(1,4,5)P_3 binding protein, in Ins(1,4,5)P_3-mediated Ca^{2+} signaling. J Cell Physiol 2005; 202:422–433.
10. Kikuno R, Nagase T, Ishikawa K, Hirosawa M, Miyajima N, Tanaka A, Kotani H, Nomura N, Ohara O. Prediction of the coding sequences of unidentified human genes. XIV. The complete sequences of 100 new cDNA clones from brain which code for large poteins in vitro. DNA Res 1999; 6:197–205.
11. Otsuki M, Fukami K, Kohno T, Yokota J, Takenawa T. Identification and characterization of a new phospholipase C-like protein, PLC-L2. Biochem Biophys Res Commun 1999; 266:97–103.
12. Yoshimura K, Takeuchi H, Sato O, Hidaka K, Doira N, Terunuma M, Harada K, Ogawa Y, Ito Y, Kanematsu T, Hirata M. Interaction of p130 with, and consequent inhibition of, the catalytic subunit of protein phosphatase 1alpha. J Biol Chem 2001; 276:17908–17913.
13. Uji A, Matsuda M, Kukitam T, Maeda K, Kanematsu T, Hirata M. Molecules interacting with PRIP-2, a novel Ins(1,4,5)P_3 binding protein type2: comparison with PRIP-1. Life Sci 2002; 72:443–453.
14. Terunuma M, Jang IS, Ha SH, Kittler JT, Kanematsu T, Jovanovic JN, Nakayama KI, Akaike N, Ryu SH, Moss SJ, Hirata M. $GABA_A$ receptor phospho-dependent modulation is regulated by phospholipase C-related inactive protein type 1, a novel protein phosphatase 1 anchoring protein. J Neurosci 2004; 24:7074–7084.
15. Kanematsu T, Yasunaga A, Mizoguchi Y, Kuratani A, Kittler JT, Jovanovic JN, Takenaka K, Nakayama KI, Fukami K, Takenawa T, Moss SJ, Nabekura J, Hirata M. Modulation of $GABA_A$ receptor phosphorylation and membrane trafficking by phospholipase C-related inactive protein/protein phosphatase 1 and 2A signaling complex underlying brain-derived neurotrophic factor-dependent regulation of GABAergic inhibition. J Biol Chem 2006; 281:22180–22189.
16. Kanematsu T, Jang IS, Yamaguchi T, Nagahama H, Yoshimura K, Hidaka K, Matsuda M, Takeuchi H, Misumi Y, Nakayama K, Yamamoto T, Akaike N, et al. Role of the PLC-related, catalytically inactive protein p130 in $GABA_A$ receptor function. EMBO J 2002; 21:1004–1011.
17. Wang H, Bedford FK, Brandon NJ, Moss SJ, Olsen RW. $GABA_A$-receptor-associated protein links $GABA_A$ receptors and the cytoskeleton. Nature 1999; 397:69–72.
18. Mizokami A, Kanematsu T, Ishibashi H, Yamaguchi T, Tanida I, Takenaka K, Nakayama KI, Fukami K, Takenawa T, Kominami E, Moss SJ, Yamamoto T, et al. Phospholipase C-related inactive protein is involved in trafficking of gamma2 subunit-containing $GABA_A$ receptors to the cell surface. J Neurosci 2007; 27:1692–1701.
19. Schneider JE. Energy balance and reproduction. Physiol Behav 2004; 81: 289–317.
20. Richards JS. Perspective: the ovarian follicle—a perspective in 2001. Endocrinology 2001; 142:2184–2193.
21. Becker JB, Arnold AP, Berkley KJ, Blaustein JD, Eckel LA, Hampson E, Herman JP, Marts S, Sadee W, Steiner M, Taylor J, Young E. Strategies and methods for research on sex differences in brain and behavior. Endocrinology 2005; 146:1650–1673.
22. John CD, Christian HC, Morris JF, Flower RJ, Solito E, Buckingham JC. Kinase-dependent regulation of the secretion of thyrotrophin and luteinizing hormone by glucocorticoids and annexin 1 peptides. J Neuroendocrinol 2003; 15:946–957.
23. Balen AH, Tan SL, Jacobs HS. Hypersecretion of luteinizing hormone: a significant cause of infertility and miscarriage. Br J Obstet Gynaecol 1993; 100:1082–1089.
24. Tarlatzis BZ, Grimbizis G, Pournaropoulos F, Bontis J, Lagos S, Spanos E, Mantealenakis S. The prognostic value of basal luteinizing hormone: follicle stimulating hormone ratio in the treatment of patients with polycystic ovarian syndrome by assisted reproduction techniques. Hum Reprod 1995; 10:2545–2549.
25. Shoham Z, Jacobs HS, Insler V. Luteinizing hormone: its role, mechanism of action, and detrimental effects when hypersecreted during the follicular phase. Fertil Steril 1993; 59:1153–1161.
26. Lenton EA, Sexton L, Lee S, Cooke ID. Progressive changes in LH and FSH and LH: FSH ratio in women throughout reproductive life. Maturitas 1988; 10:35–43.
27. Klein NA, Battaglia DE, Fujimoto VY, Davis GS, Bremner WJ, Soules MR. Reproductive aging: accelerated ovarian follicular development associated with a monotropic follicle-stimulating hormone rise in normal older women. J Clin Endocrinol Metab 1996; 81:1038–1045.
28. van Zonneveld P, Scheffer GJ, Broekmans FJ, Blankenstein MA, de Jong FH, Looman CW, Habbema JD, te Velde ER. Do cycle disturbances explain the age-related decline of female fertility? Cycle characteristics of women aged over 40 years compared with a reference population of young women. Hum Reprod 2003; 18:495–501.
29. Reame NE, Wyman TL, Phillips DJ, de Kretser DM, Padmanabhan V. Net increase in stimulatory input resulting from a decrease in inhibin B and an increase in activin A may contribute in part to the rise in follicular phase follicle-stimulating hormone of aging cycling women. J Clin Endocrinol Metab 1998; 83:3302–3307.
30. Collett ME, Wertenberger GE, Fiske VM. The effect of age upon the pattern of the menstrual cycle. Fertil Steril 1954; 5:437–448.
31. Treloar AE, Boynton RE, Behn BG, Brown BW. Variation of the human menstrual cycle through reproductive life. Int J Fertil 1967; 12:77–126.
32. DeFazio RA, Heger S, Ojeda SR, Moenter SM. Activation of A-Type-aminobutyric acid receptors excites gonadotropin-releasing hormone neurons. Mol Endocrinol 2002; 16:2872–2891.
33. Kanematsu T, Mizokami A, Watanabe K, Hirata M. Regulation of $GABA_A$-receptor surface expression with special reference to the involvement of GABARAP ($GABA_A$ receptor-associated protein) and PRIP (phospholipase C-related, but catalytically inactive protein). J Pharmacol Sci 2007; 104:285–292.
34. Stojilkovic SS, Reinhart J, Catt KJ. Gonadotropin-releasing hormone receptors: structure and signal transduction pathways. Endocr Rev 1994; 15:462–499.
35. Hille B, Tse A, Tse FW, Bosma MM. Signaling mechanisms during the response of pituitary gonadotropes to GnRH. Recent Prog Horm Res 1995; 50:75–95.
36. Kaiser UB, Conn PM, Chin WW. Studies of gonadotropin-releasing hormone (GnRH) action using GnRH receptor-expressing pituitary cell lines. Endocr Rev 1997; 18:46–70.
37. Sealfon SC, Weinstein H, Millar RP. Molecular mechanisms of ligand interaction with the gonadotropin-releasing hormone receptor. Endocr Rev 1997; 18:180–205.
38. Kile JP, Nett TM. Differential secretion of follicle-stimulating hormone and luteinizing hormone from ovine pituitary cells following activation of protein kinase A, protein kinase C, or increased intracellular calcium. Biol Reprod 1994; 50:49–54.
39. Pawson AJ, McNeilly AS. The pituitary effects of GnRH. Anim Reprod Sci 2005; 88:75–94.
40. McNeilly AS, Crawford JL, Taragnat C, Nicol L, McNeilly JR. The differential secretion of LH and FSH: regulation through genes, feedback and packaging. Reprod Suppl 2003; 61:463–476.
41. Doira N, Kanematsu K, Matsuda M, Takeuchi H, Nakano H, Ito Y, Nakayama K, Nakayama KI, Hirata M. Hyperinsulinemia in PRIP-1 gene deleted mice. Biomed Res 2001; 22:157–165.
42. Jahn R, Lang T, Südhof TC. Membrane fusion. Cell 2003; 112:519–533.

43. Südhof TC. The synaptic vesicle cycle. Ann Rev Neurosci 2004; 27:509–547.
44. Jones S, Richardson CJ, Litt RJ, Segev N. Identification of regulators for Ypt1 GTPase nucleotide cycling. Mol Biol Cell 1998; 9:2819–2837.
45. Walent J, Porter BW, Martin TFJ. A novel 145 kd brain cytosolic protein reconstitutes Ca^{2+}-regulated secretion in permeable neuroendocrine cells. Cell 1992; 70:765–775.
46. Hay JC, Martin TFJ. Resolution of regulated secretion into sequential MgATP-dependent and calcium-dependent stages mediated by distinct cytosolic proteins. J Cell Biol 1992; 119:139–151.
47. Grishanin RN, Kowalchyk JA, Klenchin VA, Ann K, Earles CA, Chapman ER, Gerona RR, Martin TF. CAPS acts at a prefusion step in dense-core vesicle exocytosis as a PIP2 binding protein. Neuron 2004; 43: 551–562.
48. Fujita Y, Ainan X, Li X, Arunachalam L, Chou TC, Jiang T, Chiew SK, Kourtesis J, Wang L, Gaisano HY, Sugita S. Ca^{2+}-dependent activator protein for secretion 1 is critical for constitutive and regulated exocytosis but not for loading of transmitters into dense core vesicles. J Biol Chem 2007; 282:21392–21403.
49. Coudevylle N, Montaville P, Leonov A, Zweckstetter M, Becker S. Structural determinants for Ca^{2+} and PIP_2 binding by the C2A domain of rabphilin-3A. J Biol Chem 2008; 283:35918–35928.
50. Montaville P, Coudevylle N, Radhakrishnan A, Leonov A, Zweckstetter M, Becker S. The PIP_2 binding mode of the C2 domains of rabphilin-3A. Protein Sci 2008; 17:1025–1034.
51. Mann RJ, Keri RA, Nilson JH. Transgenic mice with chronically elevated luteinizing hormone are infertile due to anovulation, defects in uterine receptivity, and midgestation pregnancy failure. Endocrinology 1999; 140: 2592–2601.

UICC
global cancer control

IJC
International Journal of Cancer

Loss of FBXW7, a cell cycle regulating gene, in colorectal cancer: clinical significance

Masaaki Iwatsuki[1,2], Koshi Mimori[1], Hideshi Ishii[1], Takehiko Yokobori[1], Yasushi Takatsuno[1], Tetsuya Sato[3], Hiroyuki Toh[3], Ichiro Onoyama[4], Keiichi I. Nakayama[4], Hideo Baba[2] and Masaki Mori[1]

[1] Department of Surgical Oncology, Medical Institute of Bioregulation, Kyushu University, Beppu, Japan
[2] Department of Gastroenterological Surgery, Graduate School of Medical Sciences, Kumamoto University, Kumamoto, Japan
[3] Division of Bioinformatics, Medical Institute of Bioregulation, Kyushu University, Fukuoka, Japan
[4] Department of Molecular and Cellular Biology, Division of Cell Biology, Medical Institute of Bioregulation, Kyushu University, Fukuoka, Japan

This study focused on a cell cycle regulatory gene, *FBXW7*, which ubiquitinates c-Myc and cyclin E and promotes exit from the cell cycle. We determined the expression level of *FBXW7* in colorectal cancer (CRC) cases, correlated those values with clinicopathologic features, and characterized the molecular mechanism of reduced expression of *FBXW7* in CRC cells *in vitro*. *FBXW7* mRNA and protein expression were evaluated in 93 CRC cases. Using CGH array, the copy number aberrations of the flanking region of *FBXW7* were evaluated in another 130 CRC specimens. *In vitro* analysis of *FBXW7* gene silencing in CRC cells was conducted. *FBXW7* mRNA expression was significantly lower in tumor tissues than the corresponding normal tissues. The low *FBXW7* expression group showed a significantly poorer prognosis than patients in the high expression group. A concordant relationship was observed between the incidence of *FBXW7* repression and the genetic alteration. The incidence of genetic alteration was associated with the stage of disease progression. *In vitro*, *FBXW7*-specific siRNA enhanced expression of c-MYC and cyclin E proteins and up-regulated cell proliferation. Genetic alterations in tumors led to the loss of *FBXW7* expression and increased cell proliferation. *FBXW7* expression provides a prognostic factor for patients with CRC.

Cancer Cell Biology

Normal cell growth and differentiation require appropriate regulation of the cell cycle. Deregulated cell cycle control is a fundamental aspect of cancer, resulting from mutation, deletion and transcriptional repression of genes such as pRB, and p53. Ubiquitin-mediated proteolysis is known to regulate the degradation of many proteins involved in the control of cell differentiation and growth.[1] Skp2 and FBXW7, F-box proteins containing components of the Skip1-Cull-F-box (SCF) ubiquitin ligase complexes, have been well characterized and shown to play important roles in degradation of proteins regulating cell cycle progression. Therefore, the altered expression of *FBXW7* is recognized to be one of the major causes of carcinogenesis or cancer development.[2–4] We have been focusing on expression of these cell cycle regulating genes in breast and gastric cancer.[5] In the current study, we examined FBXW7 which promotes the degradation of cyclin E, c-Myc, c-Jun and Notch and thereby negatively regulates these key oncoproteins.[6]

In an animal model, Onoyama *et al.* demonstrated conditional inactivation of Fbw7 in the T cell lineage of mice which later manifested thymic hyperplasia and eventually developed thymic lymphoma.[7] These results showed that FBXW7 plays an important role in malignant alterations of solid tumors. Thus far, there have been few studies regarding the clinicopathologic significance of *FBXW7* expression in human colorectal cancer (CRC).

In the present study, we examined copy number aberrations of *FBXW7* in a series of 130 CRC specimens using laser microdissection and a comprehensive genome hybridization (CGH) array. Then, we investigated *FBXW7* gene expression in another subset of 93 CRC samples with well-known clinicopathologic characteristics, including prognosis. The clinicopathologic significance of FBXW7 loss was validated biologically by CRC cell lines using siRNA interference.

Key words: FBXW7, colorectal cancer, c-Myc, cyclin E, CGH array
Additional Supporting Information may be found in the online version of this article.
Grant sponsor: CREST, Japan Science and Technology Agency (JST) and Japan Society for the Promotion of Science (JSPS) Grant-in-Aid for Scientific Research; **Grant numbers:** 17109013, 18659384, 18390367, 18590333, 18015039, 19591509, 19390336, 20390360, 20591547, 20790961, 20790960; **Grant sponsor:** The Ministry of Education, Culture, Sports, Science and Technology (MEXT) Grant-in-Aid for Scientific Research on Priority Areas; **Grant number:** 18015039; **Grant sponsor:** Third Term Comprehensive Ten-year Strategy for Cancer Control; **Grant number:** 16271201; **Grant sponsor:** New Energy and Industrial Technology Development Organization (NEDO) Technological Development for Chromosome Analysis
DOI: 10.1002/ijc.24879
History: Received 5 May 2009; Accepted 18 Aug 2009; Online 8 Sep 2009
Correspondence to: Masaki Mori, Department of Surgical Oncology, Medical Institute of Bioregulation, Kyushu University, 4546 Tsurumihara, Beppu 874-0838, Japan, Fax: +81-977-27-1651, E-mail: mmori@gesurg.med.osaka-u.ac.jp

Material and Methods

Clinical samples

Ninety-three CRC patients underwent surgical treatment at the Kyushu University at Beppu and affiliated hospitals between 1993 and 1999. Resected tumor and paired nontumor tissue specimens were immediately cut from resected colon and placed in RNAlater (Takara, Japan) or embedded in Tissue Tek OCT medium (Sakura, Tokyo, Japan), or frozen in liquid nitrogen and kept at −80°C until RNA extraction. Written informed consent was obtained from all patients. The median follow-up period was 3.0 years.

Quantitative RT-PCR

The sequences of *FBXW7* mRNA primers were as follows: sense, 5′-AAA GAG TTG TTA GCG GTT CTC G-3′; antisense, 5′-CCA CAT GGA TAC CAT CAA ACT G-3′. Glyceraldehyde-3-phosphate dehydrogenase (*GAPDH*) was used as an internal control and *GAPDH* primers were as follows: sense, 5′-TTG GTA TCG TGG AAG GAC TCT A-3′; antisense, 5′-TGT CAT ATT TGG CAG GTT-3′. Real-time monitoring of PCR reactions was performed using the LightCycler™ system (Roche Applied Science, Indianapolis, IN) and SYBER-Green I dye (Roche Applied Science, Indianapolis, IN). Monitoring was performed according to the manufacturer's instructions, as described previously.[8] In brief, a master mixture was prepared on ice, containing 1 μL of cDNA, 2 μL of DNA Master SYBER-Green I mix, 50 ng of primers and 2.4 μL of 25 mM $MgCl_2$. The final volume was adjusted to 20 μL with water. After the reaction mixture was loaded into glass capillary tubes, quantitative RT-PCR was performed with the following cycling conditions: initial denaturation at 95°C for 10 min, followed by 40 cycles of 95°C for 10 sec, annealing at 62°C for 10 sec and extension at 72°C for 10 sec. After amplification, products were subjected to a temperature gradient from 67°C to 95°C at 0.2°C/sec, under continuous fluorescence monitoring, to produce a melting curve of products.

Data analysis for Quantitative RT-PCR

We used the LightCycler® Software version 3.5 program (Roche Molecular Biochemicals) to calculate the cycle numbers. After proportional baseline adjustment, the fit point method was employed to determine the cycle in which the log-linear signal was first distinguishable from the baseline. This cycle number was used as the crossing point value. A standard curve was produced by measuring the crossing point of each standard value and plotting it against the logarithmic concentration value. Concentrations of unknown samples were calculated by plotting their crossing points against the standard curve and dividing by *GAPDH* content. *GAPDH* expression levels were the same in tumor and normal tissues.

Immunohistochemistry

Immunohistochemical studies for FBXW7, c-Myc and cyclin E were performed on formalin-fixed, paraffin-embedded surgical sections obtained from 71 patients with CRC. Tissue sections were deparaffinized, soaked in 0.01 M sodium citrate buffer and boiled in a microwave for 5 min at 500 W to retrieve cell antigens. The primary mouse monoclonal antibodies against FBXW7 (Abnova Corporation, Taipei, Taiwan), mouse monoclonal antibodies against c-Myc (sc-40, Santa Cruz Biotechnology, CA) and rabbit polyclonal antibodies against Cyclin E (SC-481, Santa Cruz Biotechnology) were used at dilutions of 1:100, 1:50 and 1:50, respectively. Tissue sections were immunohistochemically stained using ENVISION reagents (ENVISION+ Dual Link System-HRP, Dako Cytomation, Glostrup, Denmark). All sections were counterstained with hematoxylin. We confirmed the specificity of antibody for *FBXW7* using by the thymus of *Fbxw7* knockout mouse established by Onoyama *et al.*[7] (Supporting Information, Fig. 4).

Laser microdissection

The tissues from another series of 130 patients with CRC were collected for laser micro-dissection (LMD). CRC tissues were microdissected using the LMD system (Leica Laser Microdissection System, Leica Microsystems, Wetzlar, Germany) as previously described.[9] For LMD, 5 μ frozen sections were fixed in 70% ethanol for 30 sec, stained with hematoxylin and eosin and dehydrated as follows: 5 sec each in 70%, 95% and 100% ethanol and a final 5 min in xylene. Sections were air-dried, then microdissected with the LMD system. Target cells were excised, at least 100 cells per section, and bound to the transfer film, and total DNA extracted.

cDNA-microarray

We used the commercially available Human Whole Genome Oligo DNA Microarray Kit (Agilent Technologies, Santa Clara, CA). A list of genes on this cDNA microarray is available from http://www.chem.agilent.com/scripts/generic.asp?lpage=5175 &indcol=Y&prodcol=Y&prodcol=N&indcol=Y&prodcol=N. Cyanine (Cy)-labeled cRNA was prepared using T7 linear amplification as described in the Agilent Low RNA Input Fluorescent Linear Amplification Kit Manual (Agilent Technologies). Labeled cRNA was fragmented and hybridized to an oligonucleotide microarray (Whole Human Genome 4 × 44K Agilent G4112F). Fluorescence intensities were determined with an Agilent DNA Microarray Scanner and were analyzed using G2567AA Feature Extraction Software Version A.7.5.1 (Agilent Technologies), which used the LOWESS (locally weighted linear regression curve fit) normalization method.[10] This microarray study followed MIAME guidelines issued by the Microarray Gene Expression Data group.[11] Further analyses were performed using GeneSpring version 7.3 (Silicon Genetics, San Carlos, CA).

Array-CGH

Array-CGH was performed using the Agilent Human Genome Microarray Kit 244K (Agilent Technologies). The array-CGH platform is a high resolution 60-mer oligonucleotides based

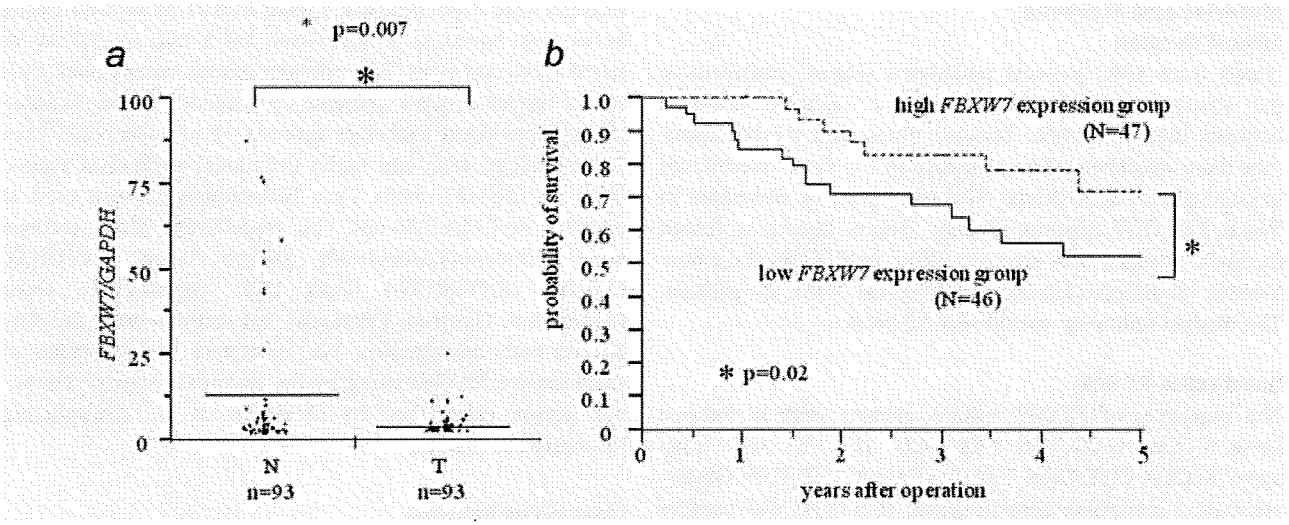

Figure 1. Clinical significance of *FBXW7* mRNA expression in CRC. (*a*) *FBXW7* mRNA expression in cancerous and normal tissues from CRC patients as assessed by real-time quantitative PCR ($n = 93$). Horizontal lines indicate mean value of each group (T, cancer tissue; N, noncancerous tissue). (*b*) Kaplan-Meier five year overall survival curves for CRC patients according to the level of *FBXW7* mRNA expression. The overall survival rate for patients in the high expression group was significantly higher than that for patients in the low expression group ($p = 0.02$). High expression group (broken line: $N = 47$), low expression group (unbroken line: $N = 46$).

microarray containing about 244,400 probes spanning coding and non-coding genomic sequences with median spacing of 7.4 kb and 16.5 kb, respectively. Labeling and hybridization were performed according to the protocol provided by Agilent (Protocol v4.0, June 2006). Arrays were analyzed using The Agilent DNA microarray scanner.

Array-CGH data analysis

The raw signal intensities of tumor DNAs were measured with Human Genome CGH Microarray 244K (Agilent Technologies) which were then transformed into log ratio to reference DNA with 'Feature Extraction' software (v9.1) of Agilent Technologies. The log ratio was thereafter used as the signal intensity of each probe. One hundred thirty samples from different patients were subjected to circular binary segmentation (CBS) after median normalization.[12] An R script written by us was used for the median normalization, whereas an R program implemented in the "DNA copy" package of the Bioconductor project (http://www.bioconductor.org) was used for the CBS analysis. Instead of all of the CGH probes, 13,403 probes from chromosome 4 (NCBI Build 35) were analyzed in this study. An absolute log2 ratio >0.263 was used as the threshold for the gain or loss in DNA copy number for each probe.

Total RNA extraction and first-strand cDNA synthesis

Frozen tissue specimens or cultured cell lines at subconfluency were homogenized, and total RNA was extracted using the modified acid-guanidine-phenol-chloroform method as described previously.[13,14] Total RNA (8.0 μg) was reverse transcribed to cDNA using M-MLV RT (Invitrogen Corp. Carlsbad, CA).

Cell lines

The human CRC cell lines, LoVo and Colo 201, were obtained from the Japanese Collection of Research Bioresoureces (JCRB, Osaka, Japan). The cell lines were maintained in Ham's F-12 medium and RPMI1640 (Invitrogen Corp.) supplemented with 10% fetal bovine serum (Equitech-Bio, Kerrville, TX), 100 units/mL penicillin G and streptomycin (Invitrogen Corp.). The cells were incubated in 5% CO_2 at 37°C and passaged every three days.

FBXW7 RNA interference

FBXW7-specific siRNA (Silencer™ Predesigned siRNA) was purchased from Ambion, USA. siRNA oligomer was diluted with Opti-MEMI® Medium without serum (Invitrogen Corp.). The diluted siRNA oligomer was mixed with the diluted Lipofectamine™ RNAiMAX (Invitrogen Corp.) and incubated for 15 min at room temperature to allow siRNA-Lipofectamine™RNAiMAX complexes to form. Diluted logarithmic growth-phase LoVo cells without antibiotics were seeded at 2×10^5 cells/well in a final volume of 2 mL or 100 μL in 6 or 96 well flat bottom microtiter plates, respectively. The cells were incubated in a humidified atmosphere (37°C and 5% CO_2). The assay was performed after 72 hr incubation.

Table 1. *FBXW7* mRNA expression and clinocopathological factors

Factors	High expression (n = 47)		Low expression (n = 46)		p value
	n	%	n	%	
Age (mean ± SD)	67.4 ± 10.0		67.4 ± 11.6		0.98
Sex					0.07
Male	30	63.8	22	47.8	
Female	17	36.2	24	52.2	
Histological grade					0.42
Well	19	40.4	14	30.4	
Moderately, poorly others	28	59.6	32	69.6	
Size					0.32
>30 mm (small)	10	21.3	11	23.9	
<31 mm (large)	37	78.7	35	76.1	
Depth of tumor invasion[1]					0.03
m, sm, sp	36	78.3	27	57.5	
s, se, si	10	22.7	20	42.5	
Lymph node metastasis					0.76
Absent	21	44.7	20	43.5	
Present	26	55.3	26	56.5	
Lymphtic invasion					0.59
Absent	29	61.7	25	54.3	
Present	18	38.3	21	45.7	
Venous invasion					0.23
Absent	43	91.5	38	82.6	
Present	4	8.5	8	17.4	
Liver metastasis					0.48
Absent	44	93.6	41	89.1	
Present	3	6.4	5	10.9	
Peritoneal dissemination					0.24
Absent	47	100.0	45	97.8	
Present	0	0.0	1	2.2	
Duke's stage					0.47
A, B	23	50.0	27	57.5	
C, D	3	50.0	20	42.5	

[1]Tumor invasion of mucosa (m), submucosa (sm), muscularis propria (mp), subserosa (ss), penetration of serosa (se), and invasion.

Western blot analysis

Total protein was extracted from cell lines using protein extraction solution (PRO-PREP, iNtRON Biotechnology, Korea). Total protein (40 μg) was electrophoresed in 10% concentrated READY GELS J (Bio-Rad Laboratories, Japan) and electroblotted onto pure nitrocellulose membranes (Trans-Blot Transfer Medium; Bio-Rad Laboratories, Japan) at 0.2 A for 120 min. c-Myc protein was detected using mouse monoclonal antibodies (sc-40, Santa Cruz Biotechnology) diluted 1:500. Cyclin E protein was detected using rabbit polyclonal antibodies (SC-481, Santa Cruz Biotechnology) diluted 1:100. c-Myc and cyclin E protein levels were normalized to the level of β-actin protein (Cytoskeleton, Denver CO) diluted 1:1,000. Blots were developed with horse-radish peroxidase-linked anti-mouse and rabbit immunoglobulin (Promega, Madison, WI) diluted 1:1,000. ECL Detection Reagents (Amersham Biosciences, Piscataway, NJ) were used to detect antigen-antibody reactions.

Proliferation assay

Proliferation of the cell lines was determined by 3-(4, 5-dimethylthiazol-2-yl)-2, 5-diphenyl tetrazolium bromide (MTT)

Table 2. Univariate and multivariate analysis for overall survival (Cox proportional regression model)

	Univariate analysis			Multivariate analysis		
Factors	**RR**	**95% CI**	***p* value**	**RR**	**95% CI**	***p* value**
Age (<65/<66)	0.820	0.540–1.218	0.328	–	–	–
Sex (male/female)	0.822	0.538–1.228	0.342	–	–	–
Histology grade (well/moderately and poorly & others)	0.690	0.416–1.063	0.095	–	–	–
Tumor size (<30 mm/>31 mm)	1.285	0.792–2.380	0.331	–	–	–
Depth of tumor invasion[1] (m, sm, mp/ss, se, si)	1.738	1.101–3.024	0.016	1.78	1.075–3.095	0.023
Lymph node metastasis(negative/positive)	2.014	1.329–3.231	0.001	2.145	1.368–3.563	0.001
Lymphatic invasion (negative/positive)	2.326	1.529–3.744	0.001	–	–	–
Venous invasion (negative/positive)	1.852	1.145–2.845	0.014	1.825	1.106–2.891	0.020
FBXW7 mRNA expression (low/high)	1.564	1.027–2.516	0.036	1.983	1.264–3.267	0.003

[1]Tumor invasion of mucosa (m), submucosa (sm), muscularis propria (mp), subserosa (ss), penetration of serosa (se), and invasion of adjacent strucures (si). Abbreviations: RR, relative risk; CI, confidence interval.

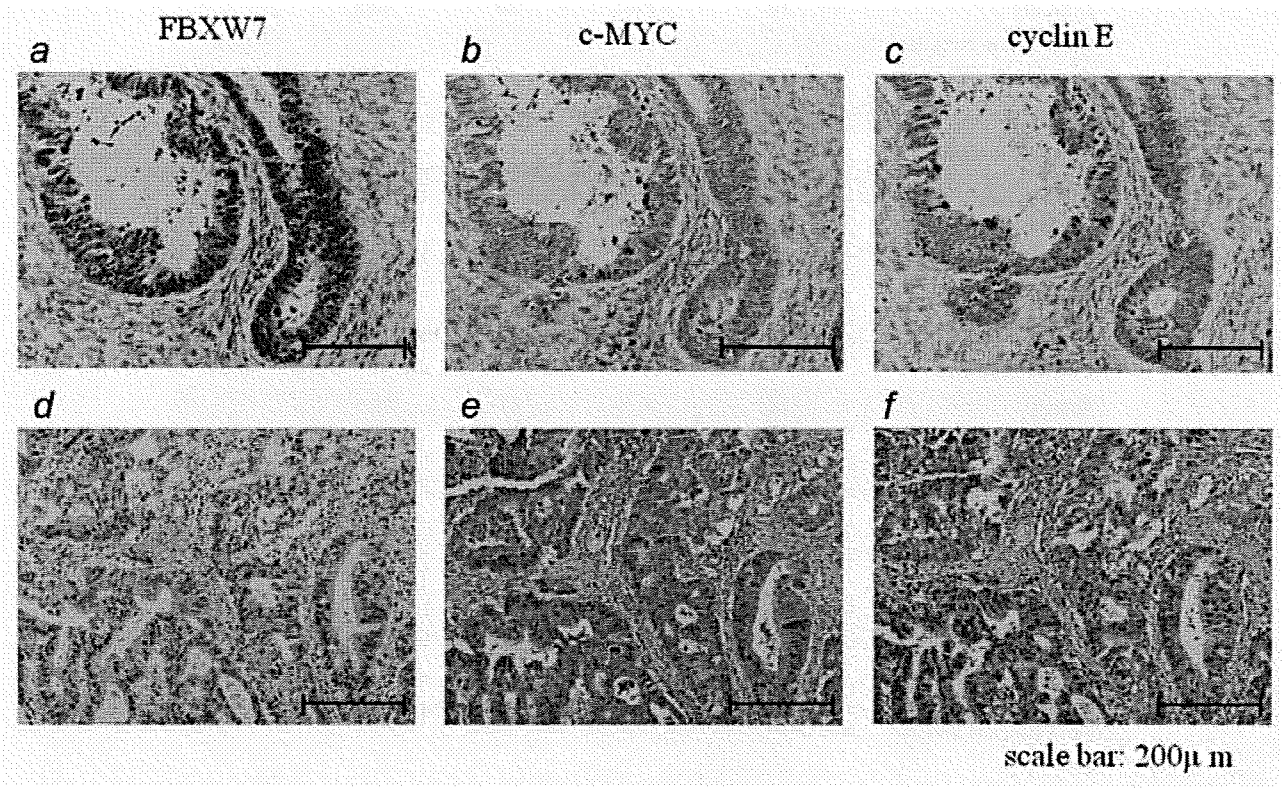

Figure 2. Immunohistochemical analysis of FBXW7, c-MYC and cyclin E expression in CRC. In cases of high FBXW7 protein expression (*a*), there was no detectable c-MYC (*b*) or cyclin E (*c*) protein expression in the same tissue section. In contrast, in the case of low FBXW7 protein expression (*d*), there was strong c-MYC (*e*) and cyclin E (*f*) protein expression (×200 original magnification). [Color figure can be viewed in the online issue, which is available at www.interscience.wiley.com.]

assay (Roche Diagnostics GmbH, Mannheim, Germany). After 24 hr incubation with siRNA, cells were seeded at 5×10^3 cells well^{-1} in microtiter plates (96 wells, flat bottom) in a final volume of 100 μL culture medium per well, in a humidified atmosphere (37°C and 5% CO_2). After 72 hr incubation, 10 μL of MTT labeling agent (final concentration 0.5 mg mL^{-1}) was added to each well. The microtiter plate was incubated for 4 hr in a humidified atmosphere. Solubilization solution (100 μL) was added to each well. The plate was allowed to stand overnight in the incubator in a

humidified atmosphere. After checking for complete solubilization of the purple formazan crystals, spectrophotometric absorbance of the sample was measured using a model 550 microplate reader (Bio-Rad Laboratories, CA), at a wavelength of 570 nm corrected 655 nm. Each independent experiment was performed three times.

Statistical analysis

For continuous variables, data were expressed as the mean ± standard deviation. The relationship between *FBXW7* mRNA expression and clinicopathological factors was analyzed using a χ^2 test and Student's *t*-test. Overall survival curves were plotted according to the Kaplan-Meier method and the generalized Log-rank test was applied to compare the survival curves. All tests were analyzed using JMP software (SAS Institute Inc., Cary, NC) and the findings were considered significant for p values <0.05.

Results

Expression of FBXW7 mRNA in clinical tissue specimens

FBXW7 mRNA expression was examined in 93 CRC clinical samples using reverse transcription-polymerase chain reaction (RT-PCR) and real-time quantitative RT-PCR, with quantified values used to calculate *FBXW7/GAPDH* ratios. In these samples, clinicopathological factors, including prognosis, were available. The mean expression level of *FBXW7* mRNA in tumor tissue specimens was significantly lower than that of nontumor tissue ($p = 0.007$) (Fig. 1*a*).

FBXW7 mRNA expression and clinicopathological characteristics

We divided the 93 CRC cases into two groups according to the median tumor (*T*)/normal (*N*) ratio of *FBXW7* mRNA expression level as determined above. Thus, 46 cases were placed in the high *FBXW7* expression group and 47 cases in the low *FBXW7* expression group. The association between clinicopathological features and *FBXW7* mRNA expression is summarized in Table 1. In the low *FBXW7* expression group, tumor invasion was significantly elevated compared to the high *FBXW7* expression group ($p = 0.02$). Univariate analysis identified *FBXW7* expression, tumor invasion, lymph node metastasis, lymphatic invasion and venous invasion as prognostic factors for 5-year overall survival following surgery. Variables with p values <0.05 by univariate analysis were selected for multivariate analysis using Cox's proportional hazards model. *FBXW7* expression [relative risk (RR): 1.98, confidence interval (CI): 1.26–3.26, $p = 0.003$] was found to be a significant factor affecting five year overall survival following surgery (Table 2). Analysis of 5-year overall survival curves showed that patients in the low *FBXW7* expression group had a significantly poorer prognosis than those in the high expression group ($p = 0.02$) (Fig. 1*b*).

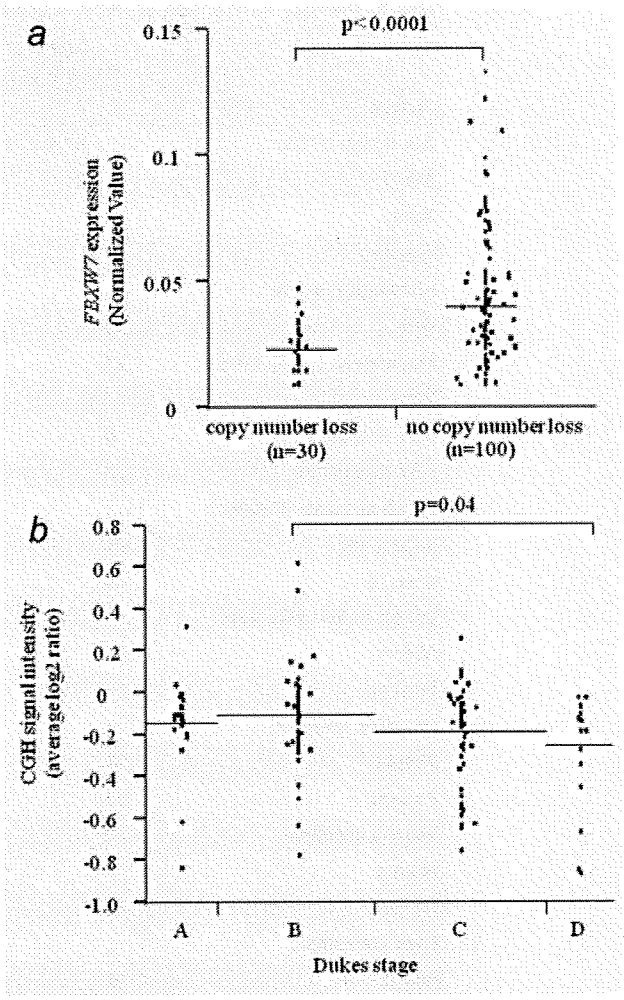

Figure 3. Concordant loss of *FBXW7* expression and copy number alteration in the flanking region of *FBXW7*. There were 30 cases with deletions and 100 cases without loss in CRC. The expression of *FBXW7* in the deleted cases was significantly lower than the cases with wild type *FBXW7* ($p < 0.0001$). (*a*) CGH signal intensity (average log2 ratio) according to Dukes staging classification. (*b*) The ratio of copy number loss of *FBXW7* increased along with the progression of Dukes' stage.

Immunohistochemical determination of FBXW7, c-MYC and cyclin E expression

Expression of FBXW7 protein was evaluated by immunohistochemistry of resected CRC specimens, using an anti-FBXW7 antibody. When FBXW7 protein was expressed at high levels, expression of c-MYC and cyclin E protein was below detection (Figs. 2*a–c*). This patient had a 5-year, recurrence-free survival after curative surgery despite the advanced stage. In contrast, in cases of low FBXW7 protein expression, strong expression of c-MYC and cyclin E proteins was noted (Figs. 2*d–f*). This patient died from peritoneal dissemination six months after curative surgery. We examined the association between *FBXW7* and *c-MYC* or *Cyclin E* in serial

Table 3. The copy number loss of *FBXW7* and clinocopathological factors

	Copy number loss group (n = 30)		No abberant group (n = 100)		
Factors	n	%	n	%	p value
Age (mean ± SD)	67.4 ± 10.0		67.4 ± 10.0		0.293
Sex					0.107
Male	13	43.3	60	60.0	
Female	17	56.7	40	40.0	
Histological grade					0.439
Well	15	50.0	58	58.0	
Moderately, poorly others	15	50.0	42	42.0	
Size					0.157
>30 mm (small)	8	26.7	15	15.0	
<31 mm (large)	22	76.3	85	85.0	
Depth of tumor invasion[1]					1.000
m, sm, sp	24	80.0	80	80.0	
s, se, si	6	20.0	20	20.0	
Lymph node metastasis					0.049
Absent	11	36.7	57	57.0	
Present	19	63.3	43	43.0	
Lymphtic invasion					0.021
Absent	8	26.7	50	50.0	
Present	22	73.3	50	50.0	
Venous invasion					0.049
Absent	7	2.3.3	42	42.0	
Present	23	76.7	58	58.0	
Liver metastasis					0.098
Absent	24	80.0	91	91.0	
Present	6	20.0	9	9.0	
Peritoneal dissemination					0.683
Absent	29	96.7	98	98.0	
Present	1	3.3	2	2.0	
Duke's stage					0.045
A, B	10	33.3	54	54.0	
C, D	20	66.7	46	46.0	

[1]Tumor invasion of mucosa (m), submucosa (sm), muscularis propria (mp), subserosa (ss), penetration of serosa (se), and invasion of adjacent strucures (si).

sections of 71 cases by immunohistochemical study. Seventy one CRC samples were divided into three groups according to *FBXW7* protein level (high = 16, medium = 19 and low = 36). We compared the expression between *FBXW7* protein and mRNA in 52 cases with high and low *FBXW7* protein level. The expression level of *FBXW7* mRNA in high *FBXW7* protein group (n = 16) is significantly higher than that in low *FBXW7* protein group (n=36) (Supporting Information 3*a*, p = 0.03). Furthermore, we found the significant inverse correlation between *FBXW7* and *c-MYC* or *cyclin E*. (supporting information, Fig. 3*b*: *FBXW vs. c-MYC*: $r = -0.526$, $p < 0.0001$, *FBXW7 vs. cyclin E*: $r = -0.553$, $p < 0.0001$).

Aberrations in FBXW7 copy number in CRC specimens

To clarify the cause of suppression of *FBXW7* mRNA in patients with poorer prognosis, we investigated copy number aberrations of *FBXW7* in 130 CRC specimens using laser micro-dissection and CGH array. As shown in Figure 3*a*, there was a significant correlation between expression of *FBXW7* and copy number of the *FBXW7* region (Fig. 3*a*) ($p < 0.0001$). Therefore, loss of *FBXW7* expression described

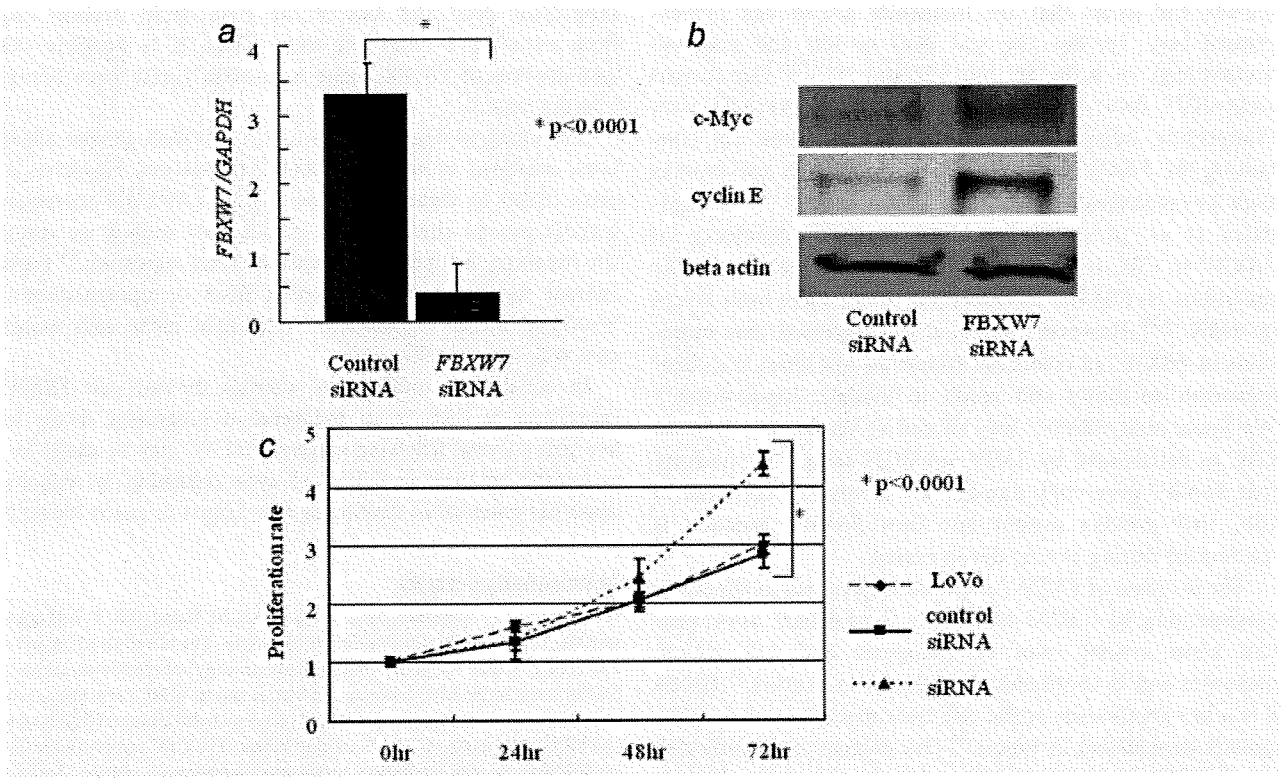

Figure 4. Effect of *FBXW7* gene silencing on a colon cancer cell line. (*a*) *FBXW7* mRNA in LoVo cells was suppressed by *FBXW7* siRNA as confirmed by quantitative RT-PCR. (*b*) Expression of c-MYC and cyclin E proteins was enhanced by *FBXW7* siRNA, as confirmed by Western blot analysis. These proteins were normalized to the level of beta actin. (*c*) The proliferation rate of LoVo cells treated with *FBXW7* siRNA (dotted line) was significantly greater than that in control siRNA cells (unbroken line) and parent LoVo cells (broken line).

above was caused by genetic alteration in the flanking region of *FBXW7*. Figure 3*b* shows CGH signal intensity (average log2 ratio) according to Dukes staging classification (Supporting Information, Fig. 1: heat map representation of copy number aberration of *FBXW7* according to Dukes staging classification). Thirty cases (23.1%) had at least one copy number aberration in all cases. The ratio of copy number loss of *FBXW7* increased along with the progression of Dukes' stage. The association between clinicopathological features and the copy number of *FBXW7* is summarized in Table 3. In the copy number loss group, lymphatic invasion, venous invasion and lymph node metastasis was increased compared with the nonaberrant group (Table 3, $p = 0.02$, $p = 0.04$ and $p = 0.04$, respectively). In addition, the copy number loss group had more advanced cases compared with the nonaberrant group ($p = 0.04$).

Effect of FBXW7 gene silencing on CRC cell lines

LoVo cells expressed *FBXW7* mRNA at a high level as confirmed by RT-PCR. We examined whether suppression of *FBXW7* would enhanced c-Myc and cyclin E protein expression, both of which are degradation targets of *FBXW7*. The expression level of *FBXW7* mRNA was suppressed by *FBXW7*-specific siRNA as confirmed by RT-PCR analysis (Fig. 4*a*). We found that the protein expression levels of c-Myc and cyclin E were enhanced by *FBXW7*-specific siRNA as confirmed by Western blotting analysis (Fig. 4*b*). Furthermore, we evaluated the proliferation activity of LoVo cells suppressed by *FBXW7*-specific siRNA using MTT assays. We found that the proliferation rate in LoVo cells suppressed by *FBXW7* siRNA significantly increased compared to that in control cells (Fig. 4*c*). We demonstrated that similar phenomena are found in Colo 201 (Supporting Information, Fig. 5).

Discussion

In our current study, we found that *FBXW7* mRNA gene expression was significantly suppressed in human CRC tissue compared to the corresponding normal tissue ($p = 0.007$) and that the patients in the low *FBXW7* expression group had a significantly poorer prognosis than those in the high expression group ($p = 0.02$). We also examined how loss of *FBXW7* contributed to cell growth.

We found that approximately 25% of patients with CRC have a reduced copy number of *FBXW7*, and that the incidence of genetic alteration was concordantly increased with the progression of disease stage. Tsafrif *et al.* and Lassmann *et al.* previously reported that particular chromosomal

regions and genes that are frequently gained and overexpressed (e.g., 7p, 8q, 13q and 20q) or lost and underexpressed (e.g., 1p, 4, 5q, 8p, 14q, 15q and 18).[15,16] Our current array-CGH data is consistent with their previous data (Supporting Information, Fig. 2). Chromosome 4q, containing the *FBXW7* gene, is deleted in various carcinomas such as esophageal, gastric, and breast cancer.[17,18] Rajagopalan *et al.* previously reported that the deficiency of *FBXW7* in CRC is associated with genetic instability.[19] The mutations in *FBXW7* in colorectal tumor have been found in 6–8%.[19,20] However, Kemp *et al.* suggested that mutations in *FBXW7* in colorectal tumor do not affect the chromosomal instability and result in biallelic inactivation.[20] We found that *FBXW7* was altered at the genetic level in CRC as determined by LMD and CGH array. Our findings that *FBXW7* gene copy number loss frequently occurred in CRC may provide insight into how *FBXW7* function is inactivated during cancer development.

The decrease of FBXW7 expression gave rise to abnormal accumulation of c-MYC and cyclin E protein.[21] MYC protein plays crucial roles in mitogenic and cell growth responses and is commonly deregulated in cancers.[22] Cyclin E is a key component of the cell cycle machinery that is frequently deregulated in cancer.[23] Our current study indicated that FBXW7 regulates c-MYC and cyclin E *in vitro*. In fact, it appears that FBXW7 normally inhibits c-Myc and cyclin E and thereby promotes exit from the cell cycle at G1-S phase. Those findings suggest that *FBXW7* may be a tumor suppressor gene and loss of the gene could prevent cells from entering a quiescent state. Thus, it is possible that introduction of *FBWX7* gene or protein could force tumors into dormancy.

According to Figure 3*a*, all CRC cases with genetic alterations exhibited diminished *FBXW7* expression. However, 65 cases (65%) in Figure 3*a* showed loss of *FBXW7* expression without genetic alteration. To explain this finding, we speculate theremay be epigenetic transcriptional regulation,[24] translational regulation by non-coding RNA or upregulation of Wnt/beta-catenin signals from interstitial niche cells associated with cancer cells.

In conclusion, multivariate analysis showed that *FBXW7* expression in CRC is an independent prognostic factor for five year survival following surgery. *FBXW7* may be useful as a prognostic indicator in CRC. Cell cycle regulation by ubiquitin ligase has potential in developing new targets in cancer therapy.

Acknowledgements

We thank Ms. T. Shimooka, Mrs. K. Ogata, Ms. M. Kasagi, Ms. Y. Nakagawa and Ms. T. Kawano for their technical assistance. The novelty and impact of this article is that we firstly investigated the copy number aberrations of FBXW7 in a series of 130 human colorectal cancer (CRC) specimens with laser microdissection by comprehensive genome hybridization (CGH) array and FBXW7 gene expression in another subset of 93 CRC samples with clinicopathlogic factors, including prognosis. Furthermore, those identified findings of the clinicopathologic significance of FBXW7 repression was validated biologically by CRC cell line with siRNA interference, which showed FBXW7 repression accelerated the cell cycle to determine a prognostic factor in CRC cases.

References

1. Bashir T, Pagano M. Aberrant ubiquitin-mediated proteolysis of cell cycle regulatory proteins and oncogenesis. *Adv Cancer Res* 2003;88:101–44.
2. Akhoondi S, Sun D, von der Lehr N, Apostolidou S, Klotz K, Maljukova A, Cepeda D, Fiegl H, Dafou D, Marth C, Mueller-Holzner E, Corcoran M, et al. FBXW7/hCDC4 is a general tumor suppressor in human cancer. *Cancer Res* 2007;67:9006–12.
3. Mao JH, Perez-Losada J, Wu D, Delrosario R, Tsunematsu R, Nakayama KI, Brown K, Bryson S, Balmain A. Fbxw7/Cdc4 is a p53-dependent, haploinsufficient tumour suppressor gene. *Nature* 2004;432:775–9.
4. Welcker M, Clurman BE. FBW7 ubiquitin ligase: a tumour suppressor at the crossroads of cell division, growth and differentiation. *Nat Rev Cancer* 2008;8:83–93.
5. Sonoda H, Inoue H, Ogawa K, Utsunomiya T, Masuda TA, Mori M. Significance of skp2 expression in primary breast cancer. *Clin Cancer Res* 2006;12:1215–20.
6. Nakayama KI, Nakayama K. Ubiquitin ligases: cell-cycle control and cancer. *Nat Rev Cancer* 2006;6:369–81.
7. Onoyama I, Tsunematsu R, Matsumoto A, Kimura T, de Alboran IM, Nakayama K, Nakayama KI. Conditional inactivation of Fbxw7 impairs cell-cycle exit during T cell differentiation and results in lymphomatogenesis. *J Exp Med* 2007;204:2875–88.
8. Ogawa K, Utsunomiya T, Mimori K, Tanaka F, Inoue H, Nagahara H, Murayama S, Mori M. Clinical significance of human kallikrein gene 6 messenger RNA expression in colorectal cancer. *Clin Cancer Res* 2005;11:2889–93.
9. Nishida K, Mine S, Utsunomiya T, Inoue H, Okamoto M, Udagawa H, Hanai T, Mori M. Global analysis of altered gene expressions during the process of esophageal squamous cell carcinogenesis in the rat: a study combined with a laser microdissection and a cDNA microarray. *Cancer Res* 2005;65:401–9.
10. Quackenbush J. Microarray data normalization and transformation. *Nat Genet* 2002;32 (Suppl):496–501.
11. Brazma A, Hingamp P, Quackenbush J, Sherlock G, Spellman P, Stoeckert C, Aach J, Ansorge W, Ball CA, Causton HC, Gaasterland T, Glenisson P, et al. Minimum information about a microarray experiment (MIAME)-toward standards for microarray data. *Nat Genet* 2001;29:365–71.
12. Venkatraman ES, Olshen AB. A faster circular binary segmentation algorithm for the analysis of array CGH data. *Bioinformatics* 2007;23:657–63.
13. Utsunomiya T, Hara Y, Kataoka A, Morita M, Arakawa H, Mori M, Nishimura S. Cystatin-like metastasis-associated protein mRNA expression in human colorectal cancer is associated with both liver metastasis and patient survival. *Clin Cancer Res* 2002;8:2591–4.
14. Utsunomiya T, Okamoto M, Hashimoto M, Yoshinaga K, Shiraishi T, Tanaka F, Mimori K, Inoue H, Watanabe G, Barnard GF, Mori M. A gene-expression signature can quantify the degree of hepatic fibrosis in the rat. *J Hepatol* 2004;41:399–406.
15. Lassmann S, Weis R, Makowiec F, Roth J, Danciu M, Hopt U, Werner M. Array CGH identifies distinct DNA copy number profiles of oncogenes and tumor

suppressor genes in chromosomal- and microsatellite-unstable sporadic colorectal carcinomas. *J Mol Med* 2007;85:293–304.
16. Tsafrir D, Bacolod M, Selvanayagam Z, Tsafrir I, Shia J, Zeng Z, Liu H, Krier C, Stengel RF, Barany F, Gerald WL, Paty PB, et al. Relationship of gene expression and chromosomal abnormalities in colorectal cancer. *Cancer Res* 2006;66:2129–37.
17. Sterian A, Kan T, Berki AT, Mori Y, Olaru A, Schulmann K, Sato F, Wang S, Paun B, Cai K, Hamilton JP, Abraham JM, et al. Mutational and LOH analyses of the chromosome 4q region in esophageal adenocarcinoma. *Oncology* 2006;70:168–72.
18. Takada H, Imoto I, Tsuda H, Sonoda I, Ichikura T, Mochizuki H, Okanoue T, Inazawa J. Screening of DNA copy-number aberrations in gastric cancer cell lines by array-based comparative genomic hybridization. *Cancer Sci* 2005;96:100–10.
19. Rajagopalan H, Jallepalli PV, Rago C, Velculescu VE, Kinzler KW, Vogelstein B, Lengauer C. Inactivation of hCDC4 can cause chromosomal instability. *Nature* 2004;428:77–81.
20. Kemp Z, Rowan A, Chambers W, Wortham N, Halford S, Sieber O, Mortensen N, von Herbay A, Gunther T, Ilyas M, Tomlinson I. CDC4 mutations occur in a subset of colorectal cancers but are not predicted to cause loss of function and are not associated with chromosomal instability. *Cancer Res* 2005;65:11361–6.
21. Welcker M, Singer J, Loeb KR, Grim J, Bloecher A, Gurien-West M, Clurman BE, Roberts JM. Multisite phosphorylation by Cdk2 and GSK3 controls cyclin E degradation. *Mol Cell* 2003;12:381–92.
22. Grandori C, Cowley SM, James LP, Eisenman RN. The Myc/Max/Mad network and the transcriptional control of cell behavior. *Annu Rev Cell Dev Biol* 2000;16:653–99.
23. Hwang HC, Clurman BE. Cyclin E in normal and neoplastic cell cycles. *Oncogene* 2005;24:2776–86.
24. Gu Z, Mitsui H, Inomata K, Honda M, Endo C, Sakurada A, Sato M, Okada Y, Kondo T, Horii A. The methylation status of FBXW7 beta-form correlates with histological subtype in human thymoma. *Biochem Biophys Res Commun* 2008;377:685–8.

THE JOURNAL OF BIOLOGICAL CHEMISTRY VOL. 285, NO. 6, pp. 3840–3849, February 5, 2010

Fbxo45, a Novel Ubiquitin Ligase, Regulates Synaptic Activity*[S]

Received for publication, July 18, 2009, and in revised form, December 1, 2009 Published, JBC Papers in Press, December 7, 2009, DOI 10.1074/jbc.M109.046284

Hirobumi Tada[‡§¶], Hirotaka James Okano[‡‖1], Hiroshi Takagi[**], Shinsuke Shibata[‡], Ikuko Yao[**], Masaki Matsumoto[‡‡§§], Toru Saiga[‡‡§§], Keiichi I. Nakayama[‡‡§§], Haruo Kashima[¶¶], Takuya Takahashi[§], Mitsutoshi Setou[‖‖2], and Hideyuki Okano[‡¶‖3]**

From the [‡]Department of Physiology, the [¶]Bridgestone Laboratory of Developmental and Regenerative Neurobiology, and the [¶¶]Department of Neuropsychiatry, Keio University School of Medicine, Tokyo 160-8582, the [§]Department of Physiology, Yokohama City University School of Medicine, Kanagawa 236-0004, [‖]SORST (Solution Oriented Research for Science and Technology) and [§§]CREST (Core Research for Evolutional Science and Technology), the Japan Science and Technology Agency, Saitama 332-0012, the [**]Laboratory for Molecular Gerontology, Mitsubishi Kagaku Institute of Life Sciences Setou Group, Tokyo 194-8511, the [‡‡]Department of Molecular and Cellular Biology, Medical Institute of Bioregulation, Kyushu University, Fukuoka 812-8582, and the [‖‖]Department of Molecular Anatomy, Hamamatsu University School of Medicine, Shizuoka 431-3192, Japan

Neurons communicate with each other through synapses. To establish the precise yet flexible connections that make up neural networks in the brain, continuous synaptic modulation is required. The ubiquitin-proteasome system of protein degradation is one of the critical mechanisms that underlie this process, playing crucial roles in the regulation of synaptic structure and function. We identified a novel ubiquitin ligase, Fbxo45, that functions at synapses. Fbxo45 is evolutionarily conserved and selectively expressed in the nervous system. We demonstrated that the knockdown of Fbxo45 in primary cultured hippocampal neurons resulted in a greater frequency of miniature excitatory postsynaptic currents. We also found that Fbxo45 induces the degradation of a synaptic vesicle-priming factor, Munc13-1. We propose that Fbxo45 plays an important role in the regulation of neurotransmission by modulating Munc13-1 at the synapse.

The nervous system stores and retrieves information via synapses, which are its primary means of communication. Synapses are specialized intercellular junctions dedicated to the transfer of information from a neuron to another neuron. Synaptic transmission is rapidly, dynamically, efficiently, and tightly regulated by several molecular mechanisms (1–4). Among these mechanisms, recent studies have shown that synaptic components are modified by protein activation (5) and degradation (6–9).

Protein degradation can be mediated by the ubiquitin-proteasome system (UPS)[4] (10–12). The modification of proteins by the ligation of ubiquitin molecules is critical role in regulating the degradation of specific proteins, thereby controlling protein turnover. This control mechanism is extremely effective because it allows the rapid elimination of particular regulatory proteins, ensuring that the biological process regulated by the proteins can be shut down immediately. Protein ubiquitination is catalyzed by a cascade of reactions involving three enzymes: E1 (ubiquitin-activating enzyme), E2 (ubiquitin-conjugating enzyme), and E3 (ubiquitin-protein ligase). E1 activates ubiquitin in an ATP-dependent reaction and transfers it to E2 with the formation of a thiol ester bond between the C terminus of ubiquitin and a cysteine residue of E2. Next, E2, either by itself or together with E3, transfers the ubiquitin moiety to a lysine residue of the substrate protein. Various E3s have been reported, and the action of each is substrate-specific. Finally, the polyubiquitinated protein is attacked by the 26S proteasome complex, which rapidly degrades it into small fragments (13).

The E3s are presently categorized into four major classes based on their specific structural motif: HECT, RING finger, U-box, and PHD-finger types (14). The RING finger-type E3s are thought to be the largest family and are further divided into subfamilies; one of these, the cullin-based E3 subfamily, is one of the largest single classes of E3. There are seven cullin-based E3s, including the Skp1-Cul1-F-box-protein (SCF) complex and the anaphase-promoting complex/cyclosome (APC/C) (14). The SCF complex E3s are composed of the scaffold protein Cul1, the RING-domain protein Rbx1/Roc1, the adaptor pro-

* This work was supported by grants from Solution-oriented Research for Science and Technology, the Japan Science and Technology Agency, the Ministry of Education, Culture, Sports, Science, and Technology (MEXT) (to Hideyuki Okano) and by grants from Japan Society for the Promotion of Science, the Keio University grant-in-aid for Encouragement of Young Medical Scientists (to H. Tada), a grant-in-aid for Scientific Research on Priority Areas (to H. J. Okano), WAKATE S and SENTAN (to M. S.), and a grant-in-aid for the Global COE program (to Keio University) from the MEXT, Japan.

[S] The on-line version of this article (available at http://www.jbc.org) contains supplemental Figs. S1–S6.

[1] To whom correspondence may be addressed: Dept. of Physiology, Keio University School of Medicine, 35 Shinanomachi, Shinjuku-ku, Tokyo 160-8582, Japan. Tel.: 81-3-5363-3747; Fax: 81-3-3357-5445; E-mail: hjokano@sc.itc.keio.ac.jp.

[2] To whom correspondence may be addressed: Dept. of Molecular Anatomy, Hamamatsu University School of Medicine, 1-20-1 Handayama, Hamamatsu, Shizuoka 431-3192, Japan. Tel. and Fax: 81-53-435-2292; E-mail: setou@hama-med.ac.jp.

[3] To whom correspondence may be addressed: Dept. of Physiology, Keio University School of Medicine, 35 Shinanomachi, Shinjuku-ku, Tokyo 160-8582, Japan. Tel.: 81-3-5363-3747; Fax: 81-3-3357-5445; E-mail: hidokano@sc.itc.keio.ac.jp.

[4] The abbreviations used are: UPS, ubiquitin-proteasome system; SCF, Skp1-Cul1-F-box-protein; PBS, phosphate-buffered saline; GFP, green fluorescent protein; DIV, days *in vitro*; siRNA, short interfering RNA; aa, amino acids; PSD, postsynaptic density; mEPSC, miniature excitatory postsynaptic current; EGFP, enhanced green fluorescent protein; HA, hemagglutinin.

tein Skp1, and one of many F-box proteins, which function to bind the substrate and constitute the largest known class of E3-specificity components. Rbx1 associates with Cul1 and E2, whereas Skp1 interacts with Cul1 and the F-box protein. The F-box protein interacts with Skp1 via its F-box motif and with substrates via its C-terminal protein-protein interaction domain (15, 16). Target molecules of several F-box proteins have been reported; for example, β-TrCP, an F-box protein that contains WD40 domain repeats, was identified as the intracellular receptor in SCF E3 for β-catenin and IκBα (17, 18); Skp2, which recognizes cyclin-dependent kinase inhibitors such as $p27^{Kip1}$, $p21^{Cip1}$, and $p57^{Kip2}$, is an F-box protein containing seven leucine-rich repeats (19).

The UPS in synaptic sites plays various roles throughout the life cycle of the synapse, *i.e.* in synaptic development, maintenance, and plasticity (6). Genetic studies in *Drosophila* and *Caenorhabditis elegans* have demonstrated the importance of E3s in synaptic development and function. For example, mutations of *highwire*, a putative E3 in *Drosophila*, or of its orthologue in *C. elegans* (*rpm-1*) lead to aberrant synaptic development (20–23). Moreover, recent studies have identified several additional mammalian E3s at the synaptic site, including SCRAPPER (9), Siah (24, 25), Staring (26), and Parkin (27). Although ample evidence supports the role of protein ubiquitination in synaptic development and plasticity in vertebrates (28), the specific molecular mechanisms underlying these effects remain to be elucidated.

Here we identified a novel synaptic E3, Fbxo45, by expression screening using the autoimmune antiserum from a patient with stomach cancer associated with psychiatric symptoms. To examine E3 functions at the synapse with potential relevance to neuronal disease, we recorded the miniature excitatory postsynaptic current (mEPSC) in hippocampal neuronal culture with or without Fbxo45. We demonstrated that Fbxo45 regulates neurotransmission at mature neurons and provides evidence that Munc13-1 may be a target or downstream molecule through which Fbxo45 acts in synaptic transmission.

EXPERIMENTAL PROCEDURES

Patient Serum and Cerebrospinal Fluid—A gastric cancer (Borrmann iv) patient showed psychiatric symptoms including severe depression, involutional melancholia, and amnesia and had high titer autoantibodies in the serum and cerebrospinal fluid, typically observed in patients with paraneoplastic neurologic disorder, a rare neurologic disorder caused by the remote effects of cancer that is thought to be immune-mediated (29, 30). Samples of the patient's serum (5 ml) and cerebrospinal fluid (3 ml) were collected. The serum and cerebrospinal fluid were spun at 15,000 × *g* for 15 min, and the supernatants were used in the following studies. All of the experimental procedures were performed with the approval of the Ethical Committee of Keio University School of Medicine.

Expression Screening—A λZAP mouse brain expression cDNA library was screened at a density of 4.5×10^5 plaque-forming units/225-mm plates. After 2 h of incubation at 42 °C, the plates were overlaid with filters soaked in 10 mM isopropyl β D-thiogalactopyranoside and incubated for 16 h at 37 °C. The plates were then cooled for 1 h at 4 °C, and the filters were removed, blocked with blocking buffer (5% skim milk and 0.5% bovine serum albumin) for 1 h, and incubated for 3 h with the patient's serum (1:500). After being washed 5 times for 6 min in washing buffer (Tris-buffered saline containing 1% Tween 20 (TBST)), the filters were incubated with horseradish peroxidase-conjugated anti-human IgG secondary antibodies (1:5000) for 1 h, and the immunoreactivities were detected using the ECL system (Amersham Biosciences).

Positive clones were purified by several rounds of antibody screening until a yield of 100% positive plaques was obtained. Phage clones were subcloned in a pBK-CMV phagemid vector using the *in vivo* excision phage rescue protocol (Stratagene).

In Situ Hybridization—Sense and antisense RNA probes (858 bp) for mouse *Fbxo45* were transcribed *in vitro* by T7 or SP6 RNA polymerase with digoxigenin-labeled UTP (Roche Applied Science). Mice were anesthetized, and the whole brain was removed. Serial frozen mouse sections (14 μm) were incubated overnight at 55 °C in a moist chamber with 200 μg of the sense or antisense probe per 50 μl of a buffer containing 50% formamide, 5× SSC (1× SSC = 0.15 M NaCl and 0.015 M sodium citrate), 50 μg/ml *Escherichia coli* tRNA, 50 μg/ml heparin sodium, and 1% SDS. The specimens were washed in 50% formamide, 5× SSC (30 min at 55 °C), 2× SSC (3 times for 30 min at 55 °C), and TBST (twice for 20 min at room temperature). After being blocked in 0.5% bovine serum albumin in TBST (60 min), the slides were incubated with an alkaline phosphatase-conjugated anti- digoxigenin antibody (Roche Applied Science) in the above buffer (overnight at 4 °C), then washed in TBST (3 times for 20 min) and NTM (100 mM NaCl, 50 mM $MgCl_2$, and 100 mM Tris-HCl, pH 9.5) for 10 min. Signals were detected in NTM containing 450 μg/ml 4-nitroblue tetrazolium chloride and 175 μg/ml 5-bromo-4-chloro-3-indolylphosphate according to the digoxigenin RNA detection kit (Roche Applied Science).

Northern Blot Analysis—Total RNAs (20 μg) from embryonic and postnatal brain and from adult mouse tissues were prepared with TRIzol reagent (Invitrogen) following the manufacturer's protocol. Purified RNAs were loaded onto a 1% formaldehyde-agarose gel after being denatured at 70 °C for 10 min. The RNAs were transferred to a nylon membrane (Amersham Biosciences) and UV-cross-linked using a Stratalinker (Stratagene). The membrane was hybridized at 51 °C with a full-length mouse *Fbxo45* or glyceraldehyde-3-phosphate dehydrogenase (*G3PDH*) cDNA probe that had been labeled with [α-^{32}P]dCTP using a Prime-It labeling kit (Stratagene). The blots were washed at 65 °C in 2, 1, and then 0.1% standard sodium citrate containing 0.1% SDS and were exposed to MR film (Eastman Kodak Co.).

Antibodies—The following antibodies were used: Synapsin-I, Munc13-1 (Synaptic Systems), synaptophysin, β-actin, FLAG, and Myc (Sigma), GFP (Wako), PSD-95 and Myc (Upstate Biotechnology), VGlut1 (Chemicon), PSD-95 (Cell Signaling), pan-Munc13, synaptotagmin, SNAP25, synaptogyrin, and Skp1 (BD Biosciences), and GFP and hemagglutinin (HA) (MBL).

To produce an anti-Fbxo45 polyclonal antibody, glutathione *S*-transferase-tagged full-length Fbxo45 (for immunohistochemistry, immunocytochemistry, and immuno-electron microscopy) or C- (257–286) terminal Fbxo45 (for immuno-

blot) bacterial fusion proteins were purified and dialyzed against PBS as described above. Rabbits were given injections of 2.5 mg of a mixture of the proteins at 3-week intervals. The antibodies were obtained by passing the serum through a column containing glutathione *S*-transferase fusion versions of the proteins.

Plasmid Construction—GFP-tagged Fbxo45 was inserted into a pEGFP-C1 vector (Clontech), and FLAG-tagged Fbxo45 and Fbxo45 deletion mutants (1–140, 54–140, and 101–286 aa) were inserted into a pFLAG-CMV-2 vector (Eastman Kodak Co.) or p3xFLAG-CMV-7.1 vector (Sigma). FLAG-Msi1, FLAG-HuC, Myc-Skp1, Myc-Munc13-1, Myc-RIM1, and HA-ubiquitin were prepared as described previously (9, 31–34, 55).

Immunoelectron Microscopy—For immunoelectron microscopic analysis, frozen sections were incubated with the anti-Fbxo45 primary antibody (1:500) followed by incubation with a nanogold-conjugated anti-rabbit secondary antibody (1:100; Invitrogen). After glutaraldehyde fixation, the signals were enhanced by a 10-min HQ-Silver kit reaction (Nanoprobes Inc.). The sections were postfixed with 0.5% osmium tetroxide, dehydrated through ethanol, and embedded in Epon. Ultrathin sections (70 μm) were cut and stained with uranyl acetate and lead citrate, observed under a transmission electron microscopy (JEOL model 1230), and photographed with a Digital Micrograph 3.3 (Gatan Inc.). For quantitative analysis, nanogold density was calculated in each neuronal compartment by counting the number of nanogold particles in every immunoelectron microscopic images using MetaMorph software (Molecular Devices, Toronto, Canada). The mean number of nanogold particles and the mean area of each compartment was measured for all discernible structures of synapse and myelin from three independent immunoelectron microscopic experiments (35).

Immunocytochemistry and Image Analysis—The cultured hippocampal neurons were prepared as described previously (9, 36). Cultured cells were fixed with 4% paraformaldehyde in PBS for 30 min at day *in vitro* (DIV) 17–18. The cells were permeabilized with 0.2% Triton X-100 for 10 min, washed with PBS, and then incubated in PBS containing TNB (PerkinElmer Life Sciences) for 1 h. The preparation was then incubated with Fbxo45 (1:100), VGlut1 (1:5000), anti-Synapsin-I (1:1000), and anti-PSD-95 (1:100) antibodies overnight at 4 °C, and after extensive washes with PBS, the preparation was overlaid with secondary antibody solution for 1 h at room temperature.

Image acquisition was performed using an LSM 510 (Carl Zeiss) and FluoView 1000 (Olympus) confocal microscope. The clusters of Synapsin-I (red)/PSD-95 (white) colocalization were counted. The red and white images were merged, the colocalized signals over the dendrites of GFP-expressing neurons were determined, and the values were entered into Microsoft Excel. The transfected neurons were chosen randomly from three independent experiments for each construct. All experiments on live animals were performed in accordance with Keio University guidelines and regulations.

Recording of the mEPSC—Cultured cells were transfected using the Lipofectamine 2000 reagent (Invitrogen) 3 days before electrophysiological analysis. For the mEPSC recording, the culture medium was replaced with a saline solution containing 168 mM NaCl, 2.4 mM KCl, 2, 5, or 10 mM $CaCl_2$, 1 mM $MgCl_2$, 10 mM glucose, 10 mM HEPES, and 0.5 μM tetrodotoxin, pH 7.3. The electrodes (5–8 MΩ) were filled with whole-cell pipette solution containing 120 mM potassium acetate, 20 mM KCl, 0.1 mM $CaCl_2$, 5 mM $MgCl_2$, 0.2 mM EGTA, 5 mM ATP, and 10 mM HEPES, pH 7.3. The whole-cell recording of GFP-expressing neurons was configured using an EPC-7 amplifier (HEKA) and a Digidata 1200 acquisition board (Axon Instruments). The membrane potential was clamped at 60 mV, and the signals were filtered at 10 kHz with the gain set at 0.5 mV/pA for 40-s recording periods. In all instances cells were excluded from analysis if a leak current >300 pA was observed. Membrane resistance (*R*m), series resistance (*R*s), and membrane capacitance (*C*m) were monitored. Only recordings with $Rm > 100$ MΩ and $Rs < 20$ MΩ were included for analysis. The mean *R*m, *R*s, and *C*m were not different ($p > 0.05$) among or within groups of cells being compared. Measurements of the frequency and amplitude of mEPSC were acquired for a period of 40 s. The mEPSC was detected by setting the amplitude threshold to the background noise level ×3 (in all electrophysiological experiments, a similar amount of data from GFP-expressing neurons transfected with each construct was acquired on the same day). The data from each neuron were then averaged and tested for statistical significance. All electrophysiological experiments were performed from at least three different platings of neurons for each of three different transfections. See our previously published method for details (5).

RNA Interference—Short interfering RNA (siRNA) duplexes for Fbxo45 were: siRNA Fbxo45-1, sense (5′-GGACCAAGAUUGGUUUCAGtt-3′) and antisense (5′-CUGAAACCAAUCUUGGUCCtt-3′); siRNA Fbxo45-2, sense (5′-GGUUUUACAUUACAUCGGAtt-3′) and antisense (5′-UCCGAUGUAAUGUAAAACCat-3′). The recommended negative control were obtained from Ambion in annealed and purified forms. Transfection of the siRNA duplexes was carried out using Lipofectamine 2000 (Invitrogen). Three microliters of Lipofectamine 2000 reagent with 100 pmol of siRNA duplex and 0.5 μg of pEGFP were transfected into cultured hippocampal neurons at DIV14. Three days after transfection, the cells were subjected to mEPSC recording.

Transfection, Immunoprecipitation, and Ubiquitination Assay—293T cells or COS cells were transfected using the FuGENE transfection reagent (Roche Applied Science) and harvested 48 h later. For the ubiquitination assay, the cells were treated with 50 μg/ml MG132 (Peptide Institute) for 3 h before they were harvested. Immunoprecipitates prepared with anti-FLAG M2 affinity gel or anti-c-Myc-agarose conjugate (Sigma) were used for immunoblotting with the appropriate antibodies.

Miscellaneous Procedures—Immunoblotting analyses were performed as described (37). The subcellular fractionation analysis of mouse brain extract was performed as described (38, 39). The stability of Munc13-1 was determined by treatment with 50 mg/ml cycloheximide (Calbiochem) for the indicated times.

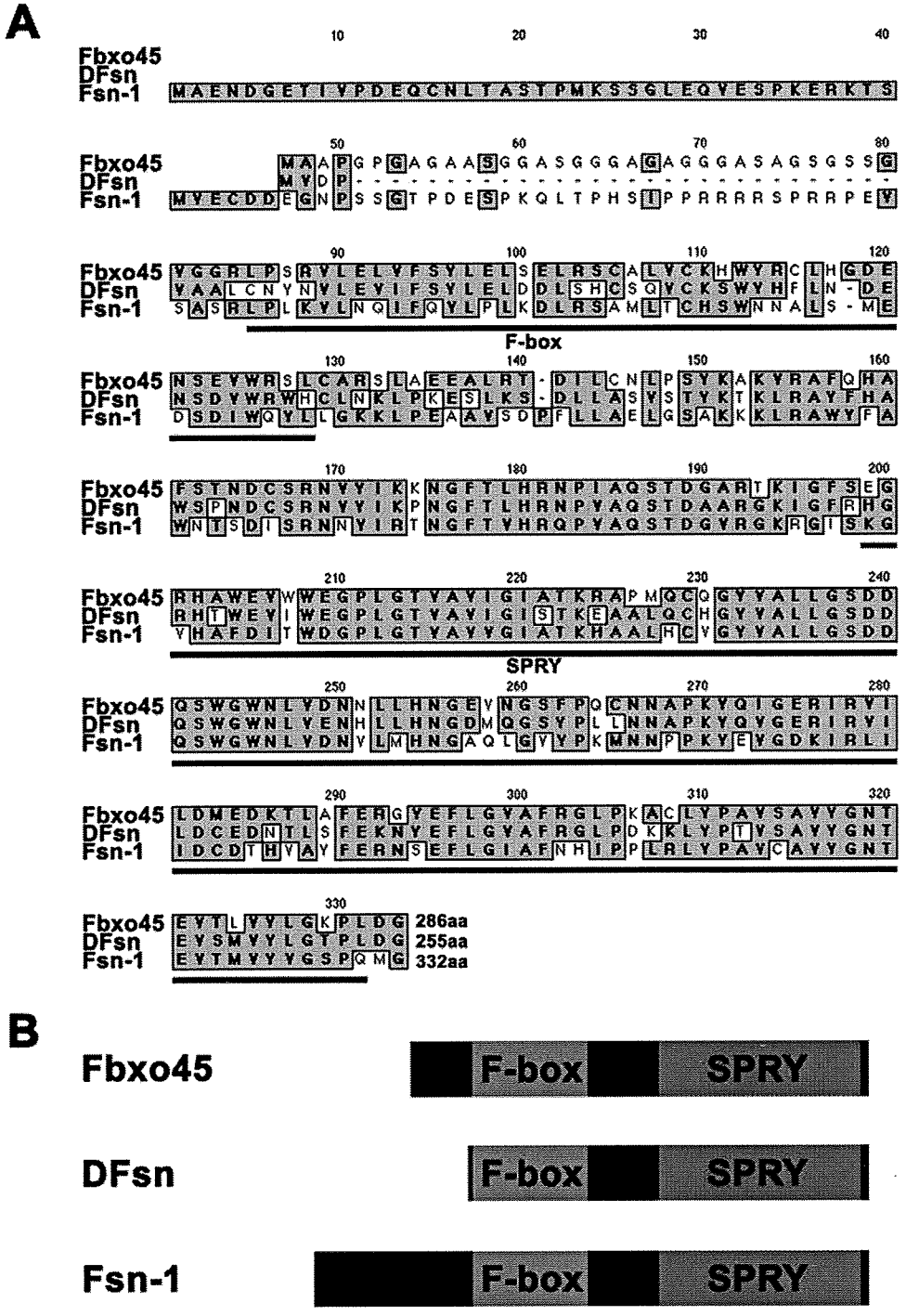

FIGURE 1. **Identification of a novel F-box protein, Fbxo45.** *A*, the amino acid sequence of mouse Fbxo45 compared with its *Drosophila* (*DFsn*) and *C. elegans* (*FSN-1*) homologues is shown. The conserved amino acids are *highlighted* in *gray*. The *underlines* indicate the signature sequences of the F-box and SPRY domains. *B*, domain structures of Fbxo45, DFsn, and FSN-1.

RESULTS

Identification of a Novel F-box Protein, Fbxo45—To identify the target molecule recognized by the autoantibody of a cancer patient with psychiatric symptoms, we performed expression screening of a mouse brain cDNA library using the patient's serum. From 1×10^6 clones screened, four positive clones were isolated. Sequence analysis showed that all four clones encoded overlapping sequences of the same cDNA, *Fbxo45*.

The *Fbxo45* gene was located on chromosome 16 in *Mus musculus* and encoded a 286-amino acid protein with an estimated molecular mass of 30 kDa. Data base (National Center for Biotechnology Information) searches with the deduced amino acid sequence of Fbxo45 revealed that it was a novel protein with striking similarity (99% identity) to a *Homo sapiens* F-box protein encoded by a gene located on chromosome 3. Recently, mammalian F-box proteins were systematically classified, and the protein corresponding to Fbxo45 was named FBXO45 (40, 41). The amino acid sequence of the Fbxo45 protein was highly conserved among species, including *Drosophila* DFsn/CG4643-PA; isoform A, CG4643-PB; isoform B (GenBank™ accession no. NP_610849, NP_725266), and *C. elegans* FSN-1 (GenBank™ accession no. NP_498046) (Fig. 1).

The deduced Fbxo45 amino acid sequence displayed some notable primary structural characteristics: an F-box domain of ~45 amino acids, located in its N-terminal region, and a SPRY (SPla and the ryanodine receptor) domain, the function of which remains unknown (42). F-box motifs are found in proteins that function as the substrate recognition component of SCF E3 complexes. The patient's autoantibodies in the serum and cerebrospinal fluid recognized the F-box domain in Fbxo45 (supplemental Fig. S1).

Tissue Distribution of Fbxo45—To elucidate the expression pattern of *Fbxo45* mRNA, we performed Northern blots, immunoblotting analyses, and *in situ* hybridization on mouse tissue preparations. The *Fbxo45* mRNA, which was ~2.7 kb, was detected preferentially in the brain at similar levels throughout development, from E12 to adulthood, and was undetectable in the tissues outside the nervous system (Fig. 2*A*). We next raised a Fbxo45-specific polyclonal antibody that recognized the 30-kDa endogenous Fbxo45 protein. Immunoblot analysis of mouse brain tissues revealed that Fbxo45 was expressed widely in the central nervous system, including the olfactory bulb, hippocampus, cortex, cerebellum, and brain stem (Fig. 3*A*, supplemental Fig. S3). *In situ* hybridization analysis showed that the

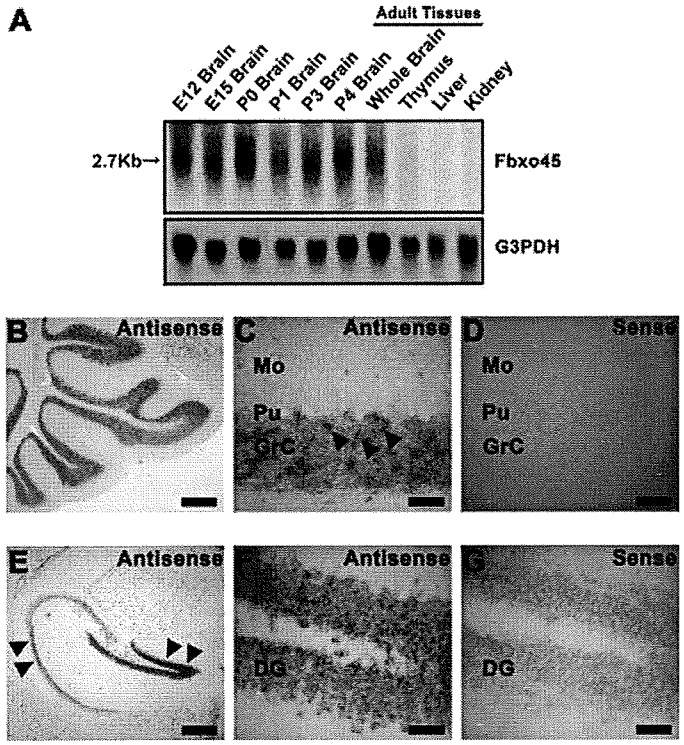

FIGURE 2. **Fbxo45 mRNA expression.** *A*, shown is a Northern blot analysis of *Fbxo45* mRNA in embryonic brain and adult tissues from mice. *G3PDH*, glyceraldehyde-3-phosphate dehydrogenase. *B–G*, shown is an *in situ* hybridization analysis of *Fbxo45* in the brain. Sagittal sections of adult mouse brain were hybridized with an antisense or sense *Fbxo45*-specific cRNA probe. *Fbxo45* expression was observed in the cerebellum (*B–D*) and hippocampus (*E–G*) as indicated by *arrowheads*. No signal was detected with the sense probe (*D* and *G*). *Mo*, Molecular layer; *Pu*, Purkinje cell layer; *GrC*, granule cell layer; *DG*, dentate gyrus. *Scale bars*: 400 μm in *B* and *E*, 50 μm in *C*, *D*, *F*, and *G*.

Fbxo45 mRNA was highly expressed in the granule cell layer of the cerebellum, dentate gyrus of the hippocampus (Fig. 2, *B–G*), granule cell layer of the olfactory bulb, and subventricular zone of the lateral ventricle (supplemental Fig. S2, *A* and *B*). It was also expressed in some cells in the cortex (supplemental Fig. S2*C*).

Expression of Fbxo45 in the Nervous System—To determine the precise location of the Fbxo45 protein in the nervous system, we examined the subcellular distribution of Fbxo45 by subcellular fractionation. Fbxo45 was enriched in the synaptic fractions, which included the synaptosomal membrane fraction (LP1), synaptic plasma membrane fraction (*SPM*), and the postsynaptic density (*PSD*) fraction (Fig. 3*B*).

We also performed immunohistochemistry using the anti-Fbxo45 polyclonal antibody, whose immunoreactivity disappeared in Fbxo45 knock-out mice (supplemental Fig. S4). Endogenous Fbxo45 protein was detected as a spotty and fibrous pattern in the primary cultured rat hippocampal neuron at DIV 16 (Fig. 3*C*). The Fbxo45 immunoreactivity was colocalized in part with a presynaptic marker, VGlut1, and a postsynaptic marker, PSD-95. Analyses using immunoelectron microscopy revealed that the significantly higher expression of Fbxo45 in both pre- and postsynaptic structures of excitatory neuron was detected compared with that in myelin cytoplasm (Fig. 3, *D* and *E*, supplemental Fig. S6). Taken together, these results support the idea that Fbxo45 could have a physiological function at the synapse.

Involvement of Fbxo45 in Neurotransmission in Rat Hippocampal Neurons—Because FSN-1, the Fbxo45 homologue in *C. elegans*, is involved in aspects of synapse formation such as the clustering of periactive zones (43), we investigated Fbxo45 involvement in synaptic function. First, we immunostained primary cultured hippocampal neurons at DIV 14 transfected with an expression vector bearing FLAG-tagged full-length Fbxo45 (FLAG-Fbxo45), vector control (FLAG-Vec), Fbxo45 siRNAs (siRNA Fbxo45-1 and -2), which significantly decreased the level of endogenous Fbxo45 protein (supplemental Fig. S5), or siRNA control (*siRNA Cont.*) for Synapsin-I and PSD-95 (Fig. 4*A*) as a marker for synapses and then evaluated whether the expression of Fbxo45 altered the number of the synapses, defined as sites in which Synapsin-I and PSD-95 were colocalized. A quantitative analysis showed no significant change in the synaptic number (Fig. 4*B*), indicating that Fbxo45 did not influence synapse formation in mature neurons.

Next, we recorded the mEPSC under whole-cell voltage clamp after blocking the sodium channel-mediated action potential activity with tetrodotoxin. Primary cultured rat hippocampal neurons at DIV 14 were transfected with Fbxo45, Fbxo45 deletion mutants (54–140 or 101–286 aa), vector control, siRNA Fbxo45-1 and -2, or siRNA control along with an EGFP-bearing vector, and the mEPSC was recorded 3 days later. We found that the knockdown of Fbxo45 significantly increased the mEPSC frequency without changing its amplitude. In contrast, the overexpression of Fbxo45 decreased the mEPSC frequency. Furthermore, a dominant-negative deletion mutant Fbxo45 (101–286 aa) lacking its F-box domain increased the mEPSC as did the siRNAs (Fig. 4, *C* and *D*). The frequency of the mEPSC was increased or decreased by the change of Fbxo45 protein level with an extracellular Ca^{2+} concentration of 2 mM; however, there was no significant difference in the mEPSC frequency compared with the control at a higher extracellular Ca^{2+} concentration (10 mM) (Fig. 4*E*). These results show that Fbxo45 functions as a negative regulator of mEPSC frequency in an extracellular Ca^{2+} concentration-dependent manner. Because Fbxo45 did not alter synapse formation in mature neurons, these findings strongly suggest that Fbxo45 regulates neurotransmission machinery.

Fbxo45 Interacts with Skp1 and Induces Protein Ubiquitination—It is known that the F-box proteins interact with an adaptor protein Skp1 and constitute the larger class of E3 specificity components. To evaluate whether Fbxo45 interacts with Skp1, we performed co-immunoprecipitation analyses. FLAG-Fbxo45, FLAG-Musashi1 (FLAG-Msi1) (31, 44), or FLAG-HuC were overexpressed in 293T cells and immunoprecipitated with a monoclonal antibody against the FLAG epitope. In the result, endogenous Skp1 was co-immunoprecipitated with overexpressed FLAG-Fbxo45 (Fig. 5*A*). The structure of Fbxo45 to form SCF complex has been described elsewhere (45).

To clarify the relationship between Fbxo45 and the ubiquitin proteolytic system, we examined whether Fbxo45 traps target proteins for the ultimate ubiquitination. Immunoblots showed multiple ubiquitinated bands of high molecular mass in the anti-FLAG immunoprecipitates from 293T cells co-transfected with FLAG-Fbxo45 and HA-tagged ubiquitin after pretreatment with the proteasome inhibitor MG132. In contrast, no